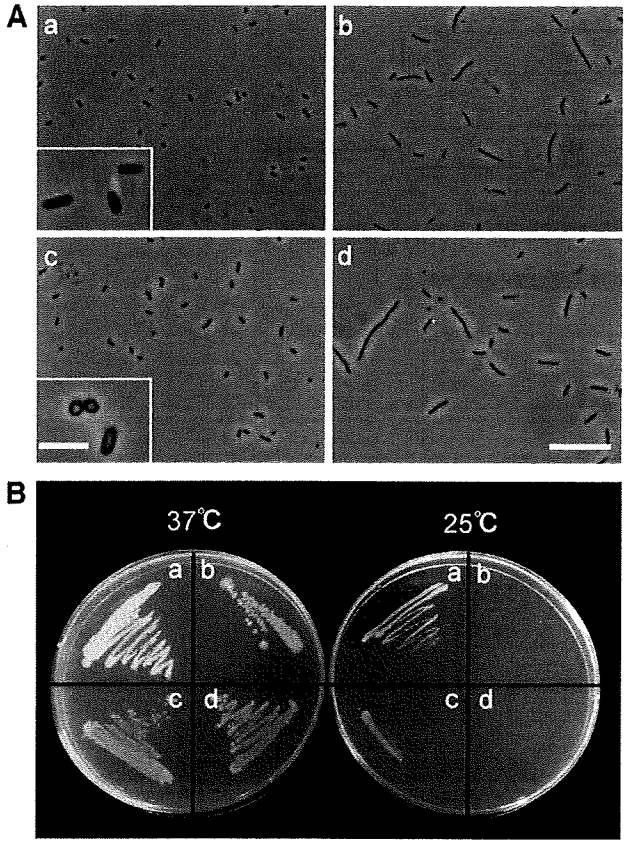

Fig. 2. PfHU complements the lack of HU in *E. coli*. (A) Phase-contrast micrographs of the HU$^+$ strain (a), the *hupAhupB* mutant (b), the *hupAhupB* mutant expressing PfHU53-189 (c) and the *hupAhupB* mutant carrying pQE50 (d). Scale bar: 5 μm. Inset, magnified view. Scale bar: 1 μm. (B) Growth of bacteria on LB plate at different temperature. Bacteria in each sector (a–d) were as in A. Each plate was incubated for 20 h (37 °C) or 40 h (25 °C).

PfHU53-189 were short in length and looked similar to the HU$^+$ parent strain (Fig 2Ac), and capable of forming robust colonies on the LB plate at both the permissive (37 °C) and the restrictive (25 °C) temperatures (Fig. 2B). The presence of the expression vector itself did not affect either the filamentous- or the cold-sensitive-phenotype of the double mutant. These results suggest that the PfHU53-189 functionally complements the deficiency of HU of the *hupAhupB* strain.

3.3. The HU gene is important for survival of the malaria parasite

Not only *P. falciparum* but other *Plasmodium* spp. have one gene for HU in the nuclear genome; for example, PB000792.02.0 (*PbHU*) is the gene of the rodent malaria parasite *P. berghei*. *Plasmodium* HUs are closely related to each other and the sequence alignment suggests that each *Plasmodium* HU has a plastid targeting sequence at the N terminus (Supplementary Fig. S4). This implies that all these *Plasmodium* HUs share the same physiological function(s). To investigate the importance of HU for *Plasmodium* spp., we constructed a targeting plasmid pPbHU-KO from pBS-DHFR [15] and attempted to disrupt the *HU* gene of *P. berghei* with the plasmid. Although the control experiment with a sister pBS-DHFR-based plasmid pPbGCS1-KO [16] easily generated the *PbGCS1* gene disruptant, we never obtained the *PbHU* knockout parasite in several repeated trials. This suggests that the *PbHU* locus is essential for the parasite's survival at least during the asexual blood stage, and that the gene is also indispensible for the survival of other species such as *P. falciparum*. Probably the HU protein encoded by the gene is important for the function and/or maintenance of the ptDNA of *Plasmodium* spp., though another possibility that the manipulation of this particular locus adversely affects the expression of other important genes [18] has not been ruled out yet.

4. Discussion

PfHU is a plastid protein and our mobility shift assay confirmed that PfHU's direct binding to the parasite's ptDNA is sequence-independent. These data imply that PfHU is involved in the assembly of the nucleoid in the plastid as an architectural protein. The filamentous phenotype of the *E. coli hupAhupB* mutant is attributed to perturbed expression of specific cell division genes [19] whereas the cold-sensitive phenotype of the mutant can be caused by unstable binding of DnaA to the binding sites in the chromosomal replication origin *oriC* [6,20]. Thus, data obtained by our complementation test suggest that PfHU adjusted the expression of genes determining bacterial shape and promoted initiation of chromosome replication by stabilising DnaA's binding to *oriC* in *E. coli*. It is questionable whether the *Plasmodium* plastid and *E. coli* share the same regulation systems for either gene expression or chromosome replication, but our data suggest that PfHU is capable to exhibits sequence-specific functions presumably by changing the architectural structure of ptDNA in the plastid.

The HU gene was impossible to knock-out from the genome of *P. berghei*, strongly suggesting that the *HU* gene is also likely indispensible for the survival of *P. falciparum*. Although it is hardly known how gene expression and replication of the organellar DNA are regulated in the *Plasmodium* plastid, PfHU is possibly involved in such sequence-dependent events in addition to general maintenance of ptDNA. Because a HU ortholog is absent from the humans, PfHU should be a promising target of the controlling drugs against malaria.

Acknowledgements

The authors thank Dr. J. Rouviere-Yaniv (Institut Pasteur, France) for providing us with *E. coli* strains JR1669, JR1670 and JR1671. This work was financially supported by the British Medical Research Council (MRC), and a Grant-in-Aid for Creative Scientific Research (18GS0314-01 to N.S. and 18GS0314 to K.K) and for Scientific Research (C) (20590426 to M.H) from Japanese Ministry of Education, Science, Culture, Sports, and Technology.

Appendix A. Supplementary data

Supplementary data associated with this article can be found, in the online version, at doi:10.1016/j.febslet.2009.03.071.

References

[1] Wilson, R.J.M. et al. (1996) Complete gene map of the plastid-like DNA of the malaria parasite *Plasmodium falciparum*. J. Mol. Biol. 261, 155–172.
[2] Ralph, S.A. et al. (2004) Tropical infectious diseases: metabolic maps and functions of the *Plasmodium falciparum* apicoplast. Nat. Rev. Microbiol. 2, 203–216.
[3] Dahl, E.L. and Rosenthal, P.J. (2008) Apicoplast translation, transcription and genome replication: targets for antimalarial antibiotics. Trends Parasitol. 24, 279–284.
[4] Sato, N., Terasawa, K., Miyajima, K. and Kabeya, Y. (2003) Organization, developmental dynamics, and evolution of plastid nucleoids. Int. Rev. Cytol. 232, 217–262.
[5] Swinger, K.K. and Rice, P.A. (2004) IHF and HU: flexible architects of bent DNA. Curr. Opin. Struct. Biol. 14, 28–35.
[6] Pettijohn, D.E. (1988) Histone-like proteins and bacterial chromosome structure. J. Biol. Chem. 263, 12793–12796.
[7] Bramhill, D. and Kornberg, A. (1988) A model for initiation at origins of DNA replication. Cell 54, 915–918.

[8] Aki, T. and Adhya, S. (1997) Repressor induced site-specific binding of HU for transcriptional regulation. EMBO J. 16, 3666–3674.
[9] Dri, A.M., Moreau, P.L. and Rouviere-Yaniv, J. (1992) Role of the histone-like proteins OsmZ and HU in homologous recombination. Gene 120, 11–16.
[10] Kobayashi, T., Takahara, M., Miyagishima, S.Y., Kuroiwa, H., Sasaki, N., Ohta, N., Matsuzaki, M. and Kuroiwa, T. (2002) Detection and localization of a chloroplast-encoded HU-like protein that organizes chloroplast nucleoids. Plant Cell 14, 1579–1589.
[11] Wu, H. and Liu, X.Q. (1997) DNA binding and bending by a chloroplast-encoded HU-like protein overexpressed in *Escherichia coli*. Plant Mol. Biol. 34, 339–343.
[12] Ram, E.V., Naik, R., Ganguli, M. and Habib, S. (2008) DNA organization by the apicoplast-targeted bacterial histone-like protein of *Plasmodium falciparum*. Nucleic Acids Res. 36, 5061–5073.
[13] Singh, D., Chaubey, S. and Habib, S. (2003) Replication of the *Plasmodium falciparum* apicoplast DNA initiates within the inverted repeat region. Mol. Biochem. Parasitol. 126, 9–14.
[14] Huisman, O., Faelen, M., Girard, D., Jaffe, A., Toussaint, A. and Rouviere-Yaniv, J. (1989) Multiple defects in *Escherichia coli* mutants lacking HU protein. J. Bacteriol. 171, 3704–3712.
[15] Dessens, J.T., Beetsma, A.L., Dimopoulos, G., Wengelnik, K., Crisanti, A., Kafatos, F.C. and Sinden, R.E. (1999) CTRP is essential for mosquito infection by malaria ookinetes. EMBO J. 18, 6221–6227.
[16] Hirai, M. et al. (2008) Male fertility of malaria parasites is determined by GCS1, a plant-type reproduction factor. Curr. Biol. 18, 607–613.
[17] Wada, M., Kano, Y., Ogawa, T., Okazaki, T. and Imamoto, F. (1988) Construction and characterization of the deletion mutant of *hupA* and *hupB* genes in *Escherichia coli*. J. Mol. Biol. 204, 581–591.
[18] Patankar, S., Munasinghe, A., Shoaibi, A., Cummings, L.M. and Wirth, D.F. (2001) Serial analysis of gene expression in *Plasmodium falciparum* reveals the global expression profile of erythrocytic stages and the presence of anti-sense transcripts in the malarial parasite. Mol. Biol. Cell 12, 3114–3125.
[19] Dri, A.M., Rouviere-Yaniv, J. and Moreau, P.L. (1991) Inhibition of cell division in *hupA hupB* mutant bacteria lacking HU protein. J. Bacteriol. 173, 2852–2863.
[20] Guo, L., Katayama, T., Seyama, Y., Sekimizu, K. and Miki, T. (1999) Isolation and characterization of novel cold-sensitive *dnaA* mutants of *Escherichia coli*. FEMS Microbiol. Lett. 176, 357–366.

THE JOURNAL OF BIOLOGICAL CHEMISTRY VOL. 284, NO. 46, pp. 31827–31833, November 13, 2009

Three Redox States of *Trypanosoma brucei* Alternative Oxidase Identified by Infrared Spectroscopy and Electrochemistry[S]

Received for publication, August 26, 2009, and in revised form, September 16, 2009 Published, JBC Papers in Press, September 19, 2009, DOI 10.1074/jbc.M109.059980

Amandine Maréchal[‡1], Yasutoshi Kido[§2], Kiyoshi Kita[§3], Anthony L. Moore[¶4], and Peter R. Rich[‡5]

From the [‡]Glynn Laboratory of Bioenergetics, Institute of Structural and Molecular Biology, University College London, Gower Street, London WC1E 6BT, United Kingdom, the [§]Department of Biomedical Chemistry, Graduate School of Medicine, University of Tokyo, Hongo 7-3-1, Bunkyo-ku, Tokyo 113-0033, Japan, and the [¶]Department of Biochemistry and Biomedical Sciences, School of Life Sciences, University of Sussex, Falmer, Brighton BN1 9QG, United Kingdom

Electrochemistry coupled with Fourier transform infrared (IR) spectroscopy was used to investigate the redox properties of recombinant alternative ubiquinol oxidase from *Trypanosoma brucei*, the organism responsible for African sleeping sickness. Stepwise reduction of the fully oxidized resting state of recombinant alternative ubiquinol oxidase revealed two distinct IR redox difference spectra. The first of these, signal 1, titrates in the reductive direction as an $n = 2$ Nernstian component with an apparent midpoint potential of 80 mV at pH 7.0. However, reoxidation of signal 1 in the same potential range under anaerobic conditions did not occur and only began with potentials in excess of 500 mV. Reoxidation by introduction of oxygen was also unsuccessful. Signal 1 contained clear features that can be assigned to protonation of at least one carboxylate group, further perturbations of carboxylic and histidine residues, bound ubiquinone, and a negative band at 1554 cm^{-1} that might arise from a radical in the fully oxidized protein. A second distinct IR redox difference spectrum, signal 2, appeared more slowly once signal 1 had been reduced. This component could be reoxidized with potentials above 100 mV. In addition, when both signals 1 and 2 were reduced, introduction of oxygen caused rapid oxidation of both components. These data are interpreted in terms of the possible active site structure and mechanism of oxygen reduction to water.

Mitochondria from many higher plants possess, in addition to the conventional cytochrome *c* oxidase, a second terminal oxidase that oxidizes ubiquinol (1–3). In thermogenic plants this alternative oxidase (AOX)[6] plays a key role in the release of heat for pollination purposes or for maintaining a warm environment within the flower at low ambient temperatures. In nonthermogenic plants its function is still under debate; proposed roles include maintaining tricarboxylic acid cycle turnover under high cytosolic phosphorylation potentials, defense against oxidative stress, and growth rate and energy charge homeostasis (4). AOX is also found in species of fungi, green algae, bacteria, and protozoa (5) and, more recently, in mollusks, nematodes, and chordates (6). Of particular importance, however, is its presence in pathogenic protozoa such as the blood parasite *Trypanosoma brucei* (7) and the intestinal parasite *Cryptosporidium parvum* (8, 9). *T. brucei* is a parasite that causes African sleeping sickness in humans and Nagana in livestock and is transmitted by the tsetse fly (7). The bloodstream forms of *T. brucei* appear to depend solely on its alternative oxidase (TAO) for respiration. Because the protein is absent from the mammalian host, TAO is an attractive and important chemotherapeutic target for African trypanosomiasis (7–10). In this respect it is interesting to note that ascofuranone, isolated from the pathogenic fungus *Ascochyta visiae*, specifically and potently inhibits the quinol oxidase activity of TAO (11) and rapidly kills the parasites. In addition, the chemotherapeutic efficacy of ascofuranone *in vivo* has been confirmed (12).

Compared with other respiratory chain complexes, the structure and mechanism of AOX are poorly characterized because of difficulties encountered in purification and a dearth of spectroscopic signatures. It has been proposed from sequence comparisons that AOX is a nonheme diiron carboxylate protein in which the metal atoms are ligated by glutamic acid and histidine residues within a four-helix bundle (1, 2, 13). The requirement for such a tertiary structural motif, as well as the necessary spacing between the iron-ligating amino acids, imposes considerable constraints upon overall possible three-dimensional structure and, consequently, its attachment to the membrane. The current model of the AOX, supported by mutagenesis studies, predicts a monotopic integral membrane protein (2, 13–15) associating with one leaflet of the lipid

[S] The on-line version of this article (available at http://www.jbc.org) contains supplemental Figs. S1–S3 and Table S1.

[1] Supported by a Wellcome Trust ViP award.
[2] Supported in part by Grant-in-aid for Young Scientists (B) 21790402.
[3] Supported by Creative Scientific Research Grant 18GS0314, Grant-in-aid for Scientific Research on Priority Areas 18073004 from the Japanese Society for the Promotion of Science, and a Targeted Proteins Research Program from the Japanese Ministry of Education, Science, Culture, Sports and Technology.
[4] Supported by the Biotechnology and Biological Sciences Research Council and the Prime Minister's Initiative 2 (Connect) fund for collaborative twinning with KK.
[5] Supported by Biotechnology and Biological Sciences Research Council Research Grant BB/H000097/1. To whom correspondence should be addressed. Tel.: 44-20-7679-7746; Fax: 44-20-7679-7096; E-mail: prr@ucl.ac.uk.

[6] The abbreviations used are: AOX, alternative oxidase; ATR, attenuated total reflection; δ_{ip}, in plane bending; FTIR, Fourier transform infrared; TAO, trypanosomal alternative oxidase; rTAO, recombinant TAO expressed in a heme-deficient strain of *E. coli*; ν_s and ν_{as}, symmetric and asymmetric stretching, respectively.

bilayer. Although analyses of yeast and trypanosomal enzymes have established that iron is required for activity (16, 17), early investigations of either mitochondria or partially purified protein failed to reveal spectroscopic signatures of its active site (18, 19). The first spectroscopic evidence for iron involvement was provided by Berthold *et al.* (20), who reported two EPR signals in *Escherichia coli* membranes that contained an overexpressed, truncated but active *Arabidopsis thaliana* alternative oxidase (AOX1a) fused to a maltose-binding protein. A signal around $g = 15$, observed with parallel mode EPR in reduced samples, was attributed to the diferrous state. A second signal, observed only after reaction of this state with oxygen, was assigned to a mixed valence ($Fe^{II}Fe^{III}$) form. More recently, Affourtit and Moore (21) prepared an active AOX protein from *Arum maculatum*. Parallel mode EPR studies (22) confirmed the presence of the diferrous signal in the reduced protein but attempts to generate the mixed valence signal of Berthold *et al.* (20) were not successful. Further spectroscopic tools are clearly desirable to resolve these inconsistencies, and, with this aim in mind, we report here the first electrochemical/FTIR study of a highly purified and stable preparation of recombinant AOX (rTAO) from *T. brucei*.

EXPERIMENTAL PROCEDURES

Isolation of rTAO—TAO was expressed in *E. coli* FN102 (Δ*hemA*) as described previously (23). In brief, rTAO was extracted by 1.4% (w/v) *n*-octyl-β-D-glucopyranoside, and, because rTAO was fused with an N-terminal histidine tag, solubilized rTAO was purified by cobalt affinity chromatography. The solubilized enzyme was bound to the cobalt affinity resin in the presence of detergent, and 100% of the rTAO activity was recovered from the column when *n*-octyl-β-D-glucopyranoside in the washing and elution buffers was exchanged with 0.042% (w/v) *n*-dodecyl-β-D-maltopyranoside. Finally, purified rTAO was obtained by two-step elution with 165 mM and 200 mM imidazole, which resulted in a very efficient purification of active rTAO in the presence of *n*-dodecyl-β-D-maltopyranoside (see supplemental Fig. S1). Specific activity of the final preparation was 207 μmol/min per mg using 150 μM ubiquinol-1.

ATR-FTIR Spectroscopy—Mid-IR spectra were recorded in ATR mode with a Bruker IFS/66S FTIR spectrophotometer fitted with a liquid nitrogen-cooled MCT-A detector at 4 cm^{-1} resolution, giving an accuracy of cited frequencies of ±1 cm^{-1}.

Sample Preparation—To remove the imidazole and to favor the interaction of the protein with the ATR prism surface, 100 μg of rTAO was diluted in 2.5 ml of 1 mM potassium phosphate buffer, pH/pD 7.0, and centrifuged at 450,000 × *g*, 4 °C, for 30 min. The pellet was resuspended with 2.5 ml of the same buffer and centrifuged for 15 min under the same conditions. The pellet was finally resuspended with 8 μl of 1 mM potassium phosphate, pH/pD 7.0. This solution was then quickly put on the ATR prism and dried under a nitrogen flow (4–5 min). The dried protein was rewetted with 10 μl of a 1 mM potassium phosphate buffer, pH/pD 7.0. The protein sample was stable with an amide II band intensity of 0.1–0.2.

Electrochemically Induced Spectroscopy—An ATR-FTIR-compatible cell with a platinum mesh working electrode was built on top of the sample layer. It was connected via a Vycor frit to a platinum sheet counter and Ag/AgCl reference electrodes (24). The chamber was filled with a freshly prepared mediator solution, and the sample was allowed to equilibrate for 1 h before starting any redox experiment. Buffer alone was placed in the reference/counter electrode chamber. All of the potential values are quoted relative to the normal hydrogen electrode.

Reduced minus oxidized spectra were induced electrochemically in 100 mM potassium phosphate, 100 mM KCl at pH/pD 7.0 and containing 500 μM potassium ferricyanide and 100 μM benzyl viologen as redox mediators. Working electrode potentials were +550 mV for oxidation and −400 mV for reduction. IR difference spectra were measured by recording a background spectrum (500 interferograms) at one potential, then switching to the second potential and recording a sample spectrum after a 13-min equilibration. Redox cycles were repeated 40 times in H_2O buffer (30 times in D_2O buffer), and reductive and oxidative spectra were averaged to produce the redox spectra shown.

For redox titration experiments, two different mixtures of mediators in 100 mM potassium phosphate, 100 mM KCl at pH 7.0 were tested: (i) 200 μM indigo trisulfonate ($n = 2$; $E_0' = -81$ mV) + 200 μM ruthenium hexamine ($n = 1$; $E_0' = +20$ mV) + 200 μM 2,4-naphthoquinone disulfonic acid ($n = 2$; $E_0' = +120$ mV) or (ii) 200 μM indigo trisulfonate + 200 μM 2,4-naphthoquinone disulfonic acid + 200 μM phenazine methosulfate ($n = 2$; $E_0' = +80$ mV) + 100 μM gallocyanine ($n = 2$; $E_0' = +20$ mV) + 1 mM ferricyanide ($n = 1$; $E_0' = +430$ mV). IR difference spectra were measured against a background spectrum of the fully oxidized (air-oxidized) sample. Reductive potentials between +200 mV and −100 mV were applied, and 15–20 min were required between two potential steps to achieve stability of the intensity of the two peak/troughs at 1658/1641 and 1544/1554 cm^{-1}. The signal amplitudes were expressed as a fraction of those of a reduced minus air-oxidized spectrum. They were plotted against potentials and simulated with the Nernstian equation,

$$y = \frac{1}{1 + \exp\left(\frac{(E_{1/2} - x) \times nF}{RT}\right)} \quad \text{(Eq. 1)}$$

where y is the oxidized fraction of TAO, x is the potential of the solution (in V), $E_{1/2}$ is the midpoint potential for the redox couple at pH 7.0, and n is the number of electrons involved in the reaction ($F = 96\,485$ C·mol^{-1}; $r = 8.314$ J·mol^{-1}·K^{-1}; $T = 298$ K). The reproducible data in Fig. 2 were obtained from a single 4-h titration.

Calculations of Vibrational Spectra—IR-active normal modes of tyrosine (Tyr-OH), tyrosinate (Tyr-O^-), and tyrosyl (Tyr-$O^\cdot$) were calculated on the UCL Legion parallel supercomputer cluster using Gaussian03 (25) with the B3LYP/6–13G(d) density functional and dataset. Data were obtained both for the zwitterionic free tyrosine as well as for tyrosine in a modified tripeptide (NH_2-Gly-Tyr-Gly-$COCH_3$) to better reflect protein environment. Molecular structures were first built with Facio (2006). Structures were then energy-minimized before calcu-

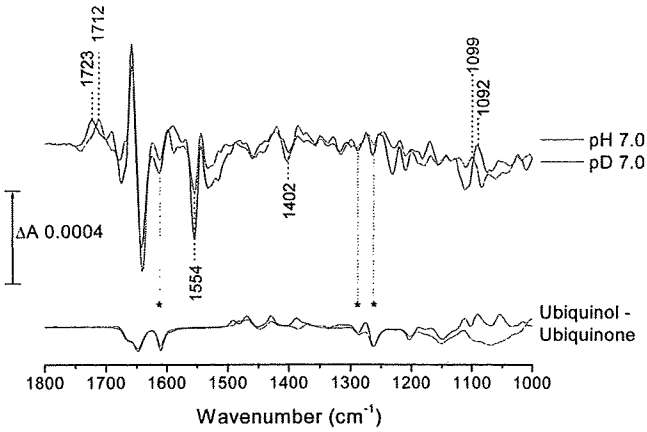

FIGURE 1. **Reduced minus oxidized IR difference spectrum of rTAO.** Reduction oxidation transformations were induced electrochemically in 100 mM potassium phosphate, 100 mM KCl at pH (*black trace*)/pD (*red trace*) 7.0 and containing 500 μM potassium ferricyanide and 100 μM benzyl viologen as redox mediators. Working electrode potentials were −400 mV for reduction and +550 mV for oxidation. For further details, see "Experimental Procedures." Published ubiquinol-10 minus ubiquinone-10 redox spectra recorded in both H_2O (*black*) and D_2O (*red*) media are also displayed for qualitative comparisons (37).

lating frequencies. Frequencies cited have been multiplied by the published scaling factor of 0.9614 (25).

RESULTS AND DISCUSSION

Secondary Structure Estimation—Information on protein secondary structure can be obtained from analyses of component bands within the amide I envelope of absolute IR absorption spectra (26, 27). Such an analysis performed on the IR spectra of rTAO in both H_2O and D_2O media predicts a minimum of 30% α-helix content in the rTAO secondary structure and up to 64% if rTAO can adopt a coiled-coil arrangement (see supplemental Table S1) (28, 29), as would occur if rTAO is folded to form the predicted four-helix bundle.

Reduced Minus Oxidized FTIR Difference Spectra—IR redox difference spectra of TAO obtained by electrochemistry at pH/pD 7.0 are shown in Fig. 1. The data were recorded in both H_2O (black) and D_2O (red) media to aid assignments. As with most redox proteins, the largest IR bands are found in the amide I (peak/trough at 1658/1641 cm^{-1}) and amide II (peak/trough at 1544/1554 cm^{-1}) regions and most commonly arise from changes in the amide I (predominantly C=O) and amide II (predominantly N–H) bands of the polypeptide backbone amide linkages. The assignment of the 1658/1641 cm^{-1} bands to redox-dependent amide I changes is strengthened by their very weak sensitivity to H/D exchange. In contrast, amide II bands are strongly shifted (≈−100 cm^{-1}) by H/D exchange, which is not the case for the 1554/1544 cm^{-1} bands. An estimation of the extent of H/D exchange from absolute IR absorption spectrum of rTAO recorded in D_2O *versus* H_2O (30) indicated that it was more than 95%. Hence, it is unlikely that the lack of shift was caused by poor H/D exchange, and other possible origins of the trough/peak at 1554/1544 cm^{-1} are discussed below.

An informative feature in the redox spectra is the positive peak at 1723 cm^{-1} in H_2O that is downshifted to 1712 cm^{-1} on H/D exchange. Bands in this frequency range with such H/D shifts are generally characteristic of protonated carboxyl groups (31, 32). There is no associated trough of equal magnitude in this region, ruling out the possibility that the carboxyl group(s) is also protonated in the oxidized state. However, a trough of roughly equal intensity was observed at 1402 cm^{-1}, slightly up-shifted (+2 cm^{-1}) on H/D exchange, together with a broad trough that underlies sharper bands in the 1560–1500 cm^{-1} amide II region. Taken together, these bands suggest the loss on reduction of the ν_s and ν_{as} vibrational modes of a deprotonated carboxylate group at 1402 and ~1530 cm^{-1} that is linked with the appearance of the 1723 cm^{-1} C=O peak of its protonated form. Hence, we conclude that reduction of rTAO results in the net protonation of one or more carboxylate groups. Deconvolution of both the H_2O and D_2O spectra with multiple Gaussian functions in the 1750-1700 cm^{-1} region (see supplemental Fig. S2) suggests that more than one carboxyl group may contribute. The best fit was obtained with two carboxyl groups being protonated (peaks at 1725 and 1717 cm^{-1} in H_2O, 1715 and 1709 cm^{-1} in D_2O) and one protonated carboxyl group changing conformation/environment on reduction (trough/peak at 1749/1735 cm^{-1} in H_2O, shifted by −8 cm^{-1} and more evident in the D_2O spectrum).

Other features around 1100 cm^{-1} are likely to arise from histidine changes (31, 33). In particular, the intense peak at 1092 cm^{-1}, upshifted to 1099 cm^{-1} in D_2O, is consistent with perturbation of an Nτ-protonated histidine bound by its Nπ to a metal center (34), as is found in the active sites of other homologous diiron proteins (35).

Finally, because reduced ubiquinone-9 is known to be the TAO electron donor in the bloodstream form of the trypanosome (36), we compared the rTAO redox spectra with published ubiquinone redox spectra recorded in both H_2O and D_2O media (37). Several bands are evident that correspond to those seen in the reference ubiquinone spectra (Fig. 1), particularly the bands at 1263 and 1289 cm^{-1} (arising from methoxy/quinone ring modes) and at 1612 cm^{-1} (from quinone C=C bonds) (38).

Redox Titration—The presence of an FTIR redox signature in rTAO provided a means to determine the redox properties of its active site by controlled potentiometry in a combined electrochemical/ATR-FTIR device (24). Redox mediators were chosen to cover the potential range from +200 to −100 mV (see "Experimental Procedures"). Fig. 2*A* presents the spectra recorded during the first reductive titration of a freshly prepared protein layer in 100 mM potassium phosphate, 100 mM KCl, at pH 7.0. The extent of reduction was estimated from the magnitudes of the two peak/troughs at 1658/1641 and 1544/1554 cm^{-1} and, typically, 15–20 min were required between two potential steps to allow their stabilization. The extent of reduction is plotted against ambient potential in Fig. 2*B*. It displayed the Nernstian behavior expected for an $n = 2$ reduction with a midpoint potential of +80 mV at pH 7.0 (see overlays in Fig. 2*B*). However, attempts to reverse the titration without hysteresis in the oxidative direction were unsuccessful, and no reoxidation was observable until potentials above +500 mV were applied (see below). Hence, it is not possible to conclude that the behavior seen in the reductive direction represents the equilibrium thermodynamic properties of this redox transition.

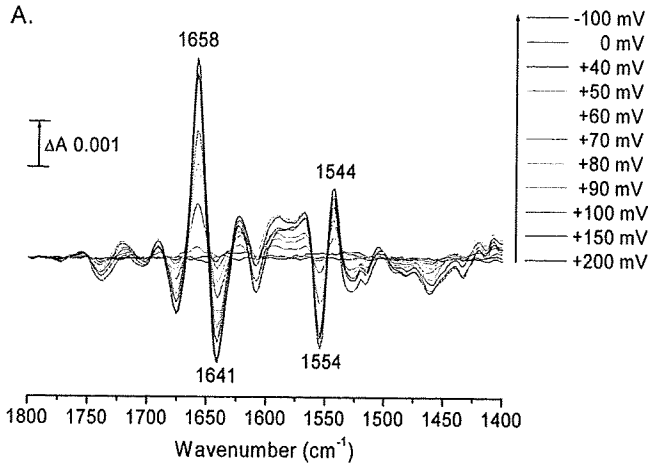

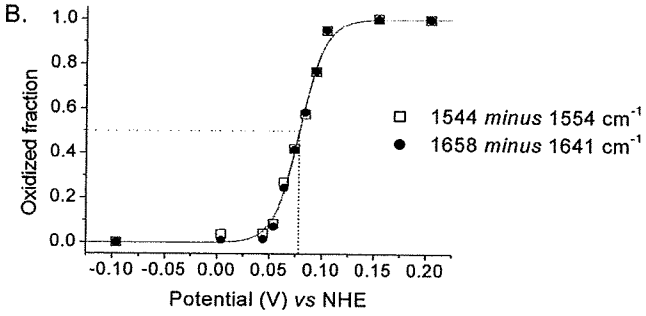

FIGURE 2. **Reductive titration of rTAO.** *A*, difference spectra recorded during a reductive titration in 100 mM potassium phosphate, 100 mM KCl at pH 7.0 (see "Experimental Procedures"). *B*, plots of peak/trough intensities at 1658/1641 and 1544/1554 cm^{-1} *versus* potential. Data were simulated with a Nernst-derived equation for an $n = 2$ component with $E_{1/2} = 79$ mV.

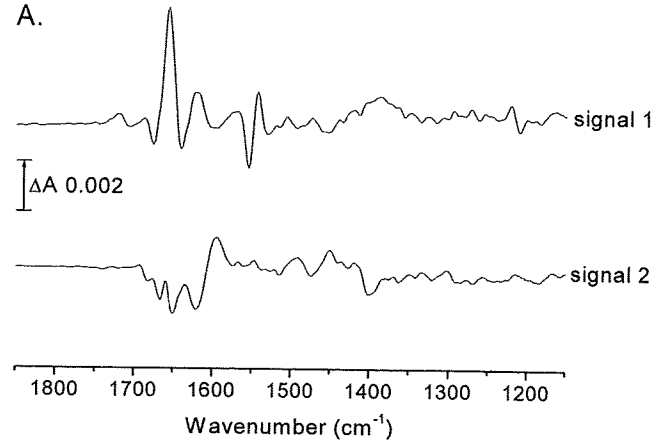

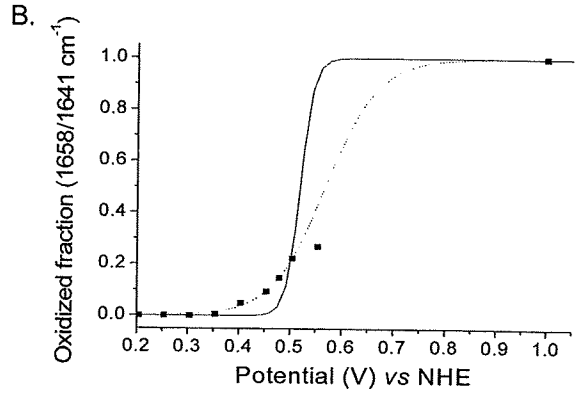

FIGURE 3. **Separation of redox spectra and oxidative titration of signal 1.** *A*, a fully oxidized spectrum was recorded and use as a background. Potential was set to −10 mV, and signal 1 was recorded after 20 min. A new background spectrum was then recorded, and signal 2 was observed to develop at 1 h. *B*, oxidative titration of signal 1 at pH 7.0 with a mixture of redox mediators containing ferricyanide. Data were simulated with a Nernst-derived equation (see "Experimental Procedures") for an $n = 2$ component with $E_{1/2} = 520$ mV (*solid line*) or for an unrestricted fit which gave $n = 0.6$ and $E_{1/2} = 510 \pm 30$ mV (*dotted line*). The maximum intensity of signal 1 was determined by the addition of dioxygen to the fully reduced state.

Introduction of oxygen into the sample when this component had become reduced also failed to promote reoxidation, indicating that this reduced state is not the oxygen-reactive species.

Further investigations revealed that there was a second redox component that was becoming reduced much more slowly than the redox component represented by the two peak/troughs at 1658/1641 and 1544/1554 cm^{-1} and termed "signal 1." This could be detected most clearly after reduction of a fully oxidized sample for 20 min at −10 mV, at which time signal 1 was fully developed and the second component remained mostly oxidized (Fig. 3*A*, *signal 1*). Maintenance of the ambient potential at −10 mV led to the appearance of a second distinct redox IR spectrum that we have termed "signal 2." Its reduction was slow (1 h at −10 mV) but, in contrast to signal 1, could be reoxidized slowly by moderate oxidizing potentials (1 h at +200 mV). A full titration of this second redox couple could not be achieved because of overlap with signal 1 and its very slow rate of redox equilibration. Nevertheless, by prereduction of both signals 1 and 2, followed by reoxidation of signal 2, a reduced minus oxidized spectrum of signal 2 alone could be obtained (Fig. 3*A*, *signal 2*), and an approximate midpoint potential around +50 mV could be estimated. Signals 1 and 2 are quite distinct components. For example, there is no signature of protonated carboxyl group at 1723 cm^{-1} or evidence of bands at 1544/1554 cm^{-1} in signal 2. These spectra are not shown below 1200 cm^{-1} because the redox mediators used also absorb in this region, and no corrections for their contributions were made.

After full reduction of both signals 1 and 2, the fully oxidized starting state of rTAO could be regenerated within the time scale of recording by introduction of O_2 into the electrochemistry cell. This contrasts markedly with the oxygen-insensitive behavior observed when only signal 1 was reduced. After reoxidation with molecular oxygen when signals 1 and 2 were reduced, signals 1 and 2 could then be titrated as before. These observations show that both redox components must be reduced to produce a form that can react with oxygen to regenerate the fully oxidized state.

In an attempt to titrate signal 1 oxidatively, redox titrations were performed with a mixture of mediators containing ferricyanide to allow equilibration at higher potentials (see "Experimental Procedures"). After full reduction of signals 1 and 2 (approximately 1.5 h at −10 mV) and oxidation of signal 2 only (approximately 1 h at +200 mV), potentials were stepped to higher values (see Fig. 3*B*). After 2.5 h with potentials as high as +550 mV, only a fraction (≈25%) of signal 1 was oxidized. We verified this was not due to protein instability by reduction back to the fully reduced form of rTAO and reintroduction of O_2, thereby regenerating 100% of the fully oxidized state. These

observations suggest that potentials in excess of +550 mV are required for full signal 1 reoxidation, which is beyond the limit of accessible electrochemistry with the platinum grid/ferricyanide system. This behavior explains the low signal amplitudes of the rTAO data of Fig. 1 because the data are an average of cyclical reductions and oxidations without introduction of oxygen to regenerate the oxidized state fully and without a very long time at reducing potentials to reduce signal 2 fully. The cycle of reduction of signal 1 and signal 2 followed by injection of O_2 into the electrochemistry cell to restore the fully oxidized resting state could be repeated reproducibly over many cycles, indicating that the enzyme itself remained very stable during the course of these investigations.

By comparison of band intensities at 1263 and 1612 cm^{-1} of a full redox spectrum of an optimized protein layer with those of a standardized solution of ubiquinone-10 in chloroform (see supplemental Fig. S3), a ubiquinone concentration in the layer was estimated to be approximately 4 mM. Previously, it has been shown that a layer of bovine cytochrome *c* oxidase (molecular mass, 204,000 Da; amide II band, approximately 0.25 ΔA) is maximally 1.8 mM (based on perfect packing) (39). Hence, the rTAO concentration (molecular mass, 34,000 Da; amide II band, 0.22 ΔA) could be up to 9 mM. As a result, it is concluded that the rTAO has retained ubiquinone such that its Q site is partially occupied with substrate ubiquinone.

Relevance to Catalytic Cycle—This study has revealed two redox processes that have distinct IR signatures, signal 1 and signal 2. Signal 1 could be titrated in the reductive direction where it behaved as if it were an $n = 2$ process with a midpoint potential of +80 mV at pH 7.0. However, the reaction was not reversible over the same potential range, indicating that this does not represent its equilibrium thermodynamic properties, a conclusion confirmed by the observation that even partial reoxidation of signal 1 could be achieved only with potentials of +550 mV. Such behavior can be observed in $n = 2$ redox systems when the one-electron intermediate is highly unstable, such as is seen, for example, in cyclic voltammetric behavior of quinones (40). In this case, reduction is controlled by the low potential reduction of quinone to semiquinone, whereas quinol oxidation is controlled by the high potential step of quinol oxidation to semiquinone. Hence, both oxidative and reductive waves appear only at overpotentials compared with the equilibrium $n = 2$ potential. It is possible that the behavior of signal 1 arises from a similar phenomenon in which it is an $n = 2$ reaction, but with a highly unstable one-electron form. In this case, the true thermodynamic $n = 2$ midpoint potential will lie somewhere between the observable reductive and oxidative waves. It is also possible that reduction of signal 1 by mediators is indirect, being mediated by the ubiquinone that is bound to the protein and that it is the known redox hysteresis of the ubiquinone that gives rise to the signal 1 behavior. A further possibility is that reduction of signal 1 induces a conformational change of the protein, raising the signal 1 potential to much higher values, a type of behavior that has been proposed to explain hysteresis of cytochrome cd_1 redox titrations (41).

Signal 2 behaves more conventionally in that it appears to be reversibly oxidized and reduced over the same potential range, with a midpoint potential around +50 mV. However, its equilibration was far too slow to be able to perform an accurate redox titration to determine whether it had an *n* value of 1 or 2. These slow kinetics are not limited by diffusion of mediators between electrode and protein layer. They most likely arise because of slow equilibration between mediators and the redox group(s) involved.

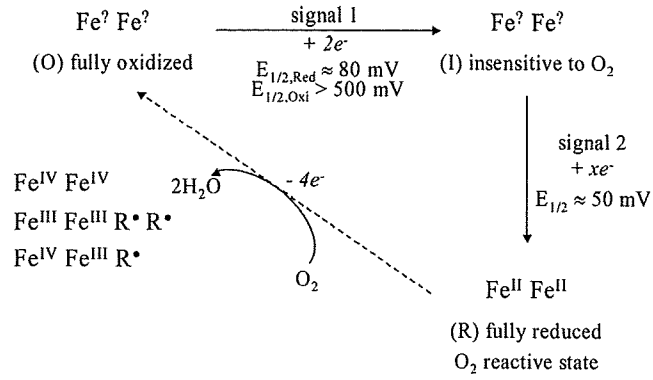

FIGURE 4. **Summary of experimental observations and their relation to the catalytic cycle of reduction of oxygen to water.**

In Fig. 4, a working model is proposed of the relationship between these IR-observed species and the physiological reaction cycle of the 4-electron reduction of dioxygen to water. Starting from the fully oxidized resting state of TAO (O), a 2-electron reduction occurs, represented by signal 1. This produces a species (I) that is insensitive to the presence of dioxygen. The (I) minus (O) IR difference spectrum shows clearly the net protonation of at least one carboxylate residue, and this is likely to give the transition a pH-dependent midpoint potential. In addition, the complexity of the carboxylic acid region changes, indicative of an additional underlying carboxylic acid shift, together with perturbations in the 1100 cm^{-1} region that indicate histidine alterations, are consistent with the proposed involvement of glutamic and histidine residues in the active site (1, 2, 13).

Species (I) can be further reduced, most probably with two electrons, to give a third redox state (R) that is the oxygen-reactive form. (R) must presumably correspond to the diferrous state that gives rise to the spin-coupled $Fe^{II}Fe^{II}$ EPR signal at $g \geq 15$ that was observed in dithionite-reduced samples by Berthold *et al.* (20) and Moore *et al.* (22). The need to reduce TAO fully to react with oxygen to form the (O) state might be related to the observation of Berthold *et al.* that an $Fe^{II}Fe^{III}$ mixed-valence state could only be observed by oxidation of the fully reduced state with oxygen (42). However, because of the differences in protocol details, it is not possible at present to determine whether the mixed-valence form should correspond to (O) or (I).

(R) can react rapidly with dioxygen to regenerate the fully oxidized (O) state. Because 4 electrons are required for reduction of dioxygen to water, the oxidation state of (O) will depend on whether the electrons are provided solely by the two metals, by protein residue(s) that produce radicals, or by substrate ubiquinol. Hence, if the (O) state does indeed result in formation of water, it must be (i) a diferryl center ($Fe^{IV}Fe^{IV}$); (ii) a diferric center plus two radicals ($Fe^{III}Fe^{III}R^{\bullet}R^{\bullet}$); (iii) a mixed-

valence ferryl/ferric center plus a radical ($Fe^{IV}Fe^{III}R^{\bullet}$) (3). All of these species are potentially EPR-silent. Such radicals could arise from amino acids or, possibly, substrate ubiquinol. Reduction of (O) to (I) most likely involves addition of two reducing equivalents into the (O) state that reduce the metals and/or radicals. Finally, it also remains possible that oxygen is incompletely reduced in the (O) state, which could, for example, contain a bound peroxide that becomes reduced in the (O) to (I) transition. Such a species could well explain the irreversibility of the reduction. However, it is difficult to reconcile a peroxide species with the formation of a mixed-valence form, and so this possibility presently seems unlikely.

In the R2 subunit of the ribonucleotide reductase, a well characterized diiron carboxylate protein, a tyrosyl residue is involved in catalysis. The fact that this residue is buried deeply into the protein structure provides it with a peculiar stability (up to several days) (43). Mutagenesis studies of both the plant AOX (44) and TAO (15) have revealed that tyrosine 275 is crucial for catalysis. This tyrosine or, possibly, a nearby tryptophan 206 (*Sauromatum guttatum* numbering) might provide a radical site (44, 45); hence a role for radical(s) in the TAO catalytic cycle seems likely. The sharp H/D-insensitive negative band at 1554 cm^{-1} could arise from the loss of a radical in the (O) to (I) transformation. Radicals of ubiquinone are expected to have a sharp band around 1490 cm^{-1}. IR and Raman features of neutral phenoxyl radical models and tyrosine radicals in proteins show two prominent modes of the neutral phenolic radical identified as ν_{8a}(C–C) at 1550–1610 cm^{-1} and ν_{7a}(C–O) at 1480–1530 cm^{-1}, and the radical state of TyrD in photosystem II shows two bands at 1551 and 1503 cm^{-1} (46–48). Moreover, density functional theory simulations (see "Experimental Procedures") of a neutral tyrosyl radical in both free zwitterionic tyrosine and in a model peptide also predict a strong band at 1554 cm^{-1}. In contrast, the rather limited IR data on tryptophanyl radicals indicate that they have IR bands at higher frequencies (49). Hence, if the 1554 cm^{-1} band does indeed arise from a radical, a tyrosyl species in the (O) state is currently most favored. Ground-state tyrosine in its protonated form is known to have bands at 1508 cm^{-1} and, in the tyrosinate form, at 1547 cm^{-1}. These bands also appear in density functional theory simulations, with an assignment to a normal mode arising from ν(C–O) + ν_s(C–C_{ring}) + δ_{IP}(H–C_{ring}). Hence, if the 1544/1554 cm^{-1} peak/trough in signal 1 does arise from tyrosine, then it most closely resembles the loss of a neutral tyrosyl radical in (O) and formation of a tyrosinate in (I) and (R). In any case, such a stable tyrosyl radical would have to be in an unusual environment in TAO, and stabilization of the tyrosinate state in (I) should make the formation of a radical energetically more facile. Further IR work on TAO and related diiron proteins, in particular a combination of FTIR and EPR analyses of the same redox states, should resolve both the nature of the mixed valence form and the involvement and types of any radicals.

REFERENCES

1. Finnegan, P. M., Soole, K. L., and Umbach, A. L. (2004) *Plant Mitochondria: From Genome To Function*, p. 163, Kluwer Academic Publishers, Dordrecht, The Netherlands
2. Berthold, D. A., and Stenmark, P. (2003) *Annu. Rev. Plant. Biol.* 54, 497–517
3. Affourtit, C., Albury, M. S., Crichton, P. G., and Moore, A. L. (2002) *FEBS Lett.* **510,** 121–126
4. Moore, A. L., Albury, M. S., Crichton, P. G., and Affourtit, C. (2002) *Trends Plant Sci.* **7,** 478–481
5. McDonald, A. E., and Vanlerberghe, G. C. (2006) *Comp. Biochem. Physiol. D* **1,** 357–364
6. McDonald, A., and Vanlerberghe, G. (2004) *IUBMB Life* **56,** 333–341
7. Chaudhuri, M., Ott, R. D., and Hill, G. C. (2006) *Trends Parasitol.* **22,** 484–491
8. Roberts, C. W., Roberts, F., Henriquez, F. L., Akiyoshi, D., Samuel, B. U., Richards, T. A., Milhous, W., Kyle, D., McIntosh, L., Hill, G. C., Chaudhuri, M., Tzipori, S., and McLeod, R. (2004) *Int. J. Parasitol.* **34,** 297–308
9. Suzuki, T., Hashimoto, T., Yabu, Y., Kido, Y., Sakamoto, K., Nihei, C., Hato, M., Suzuki, S., Amano, Y., Nagai, K., Hosokawa, T., Minagawa, N., Ohta, N., and Kita, K. (2004) *Biochem. Biophys. Res. Commun.* **313,** 1044–1052
10. Nihei, C., Fukai, Y., and Kita, K. (2002) *Biochim. Biophys. Acta* **1587,** 234–239
11. Minagawa, N., Yabu, Y., Kita, K., Nagai, K., Ohta, N., Meguro, K., Sakajo, S., and Yoshimoto, A. (1997) *Mol. Biochem. Parasitol.* **84,** 271–280
12. Yabu, Y., Yoshida, A., Suzuki, T., Nihei, C., Kawai, K., Minagawa, N., Hosokawa, T., Nagai, K., Kita, K., and Ohta, N. (2003) *Parasitol. Int.* **52,** 155–164
13. Andersson, M. E., and Nordlund, P. (1999) *FEBS Lett.* **449,** 17–22
14. Berthold, D. A., Andersson, M. E., and Nordlund, P. (2000) *Biochim. Biophys. Acta* **1460,** 241–254
15. Nakamura, K., Sakamoto, K., Kido, Y., Fujimoto, Y., Suzuki, T., Suzuki, M., Yabu, Y., Ohta, N., Tsuda, A., Onuma, M., and Kita, K. (2005) *Biochem. Biophys. Res. Commun.* **334,** 593–600
16. Minagawa, N., Sakajo, S., Komiyama, T., and Yoshimoto, A. (1990) *FEBS Lett.* **267,** 114–116
17. Ajayi, W. U., Chaudhuri, M., and Hill, G. C. (2002) *J. Biol. Chem.* **277,** 8187–8193
18. Rich, P. R. (1978) *FEBS Lett.* **96,** 252–256
19. Berthold, D. A., and Siedow, J. N. (1993) *Plant Physiol.* **101,** 113–119
20. Berthold, D. A., Voevodskaya, N., Stenmark, P., Gräslund, A., and Nordlund, P. (2002) *J. Biol. Chem.* **277,** 43608–43614
21. Affourtit, C., and Moore, A. L. (2004) *Biochim. Biophys. Acta* **1608,** 181–189
22. Moore, A. L., Carré, J. E., Affourtit, C., Albury, M. S., Crichton, P. G., Kita, K., and Heathcote, P. (2008) *Biochim. Biophys. Acta* **1777,** 327–330
23. Nihei, C., Fukai, Y., Kawai, K., Osanai, A., Yabu, Y., Suzuki, T., Ohta, N., Minagawa, N., Nagai, K., and Kita, K. (2003) *FEBS Lett.* **538,** 35–40
24. Rich, P. R., and Iwaki, M. (2007) *Mol. BioSys.* **3,** 398–407
25. Frisch, M. J., Trucks, G. W., Schlegel, H. B., Scuseria, G. E., Robb, M. A., Cheeseman, J. R., Montgomery, J. A., Jr., Vreven, T., Kudin, K. N., Burant, J. C., Millam, J. M., Iyengar, I. I., Tomasi, J., Barone, V., Mennucci, B., Cossi, M., Scalmani, G., Rega, N., Petersson, G. A., Nakasuji, H., Hada, M., Ehara, M., Toyota, K., Fukuda, R., Hasegawa, J., Ishida, M., Nakajima, T., Honda, Y., Kitao, O., Nakai, H., Klene, M., Li, X., Knox, J. E., Hratchian, H. P., Cross, J. B., Bakken, V., Adamo, C., Jaramillo, J., Gomperts, R., Stratmann, R. E., Yazyev, O., Austin, A. J., Cammi, R., Pomelli, C., Ochterski, J. W., Ayala, P. Y., Morokuma, K., Voth, G. A., Salvador, P., Dannenberg, J. J., Zakrzewski, G., Dapprich, S., Daniels, A. D., Strain, M. C., Farkas, O., Malick, D. K., Rabuck, A. D., Raghavachari, K., Foresman, J. B., Ortiz, J. V., Cui, Q., Baboul, A. G., Clifford, S., Cioslowski, J., Stefanov, B. B., Liu, G., Liashenko, A., Piskorz, P., Komaromi, I., Martin, R. L., Fox, D. J., Keith, T., Al-Laham, M. A., Peng, C. Y., Nanayakkara, A., Challacombe, M., Gill, P. M. W., Johnson, B., Chen, W., Wong, M. W., Gonzalez, C., and Pople, J. A. (2005) *Gaussian 03*, Gaussian, Inc., Wallingford, CT
26. Arrondo, J. L. R., Muga, A., Castresana, J., and Goñi, F. M. (1993) *Prog. Biophys. Mol. Biol.* **59,** 23–56
27. Arrondo, J. L. R., and Goñi, F. M. (1999) *Prog. Biophys. Mol. Biol.* **72,** 367–405
28. Heimburg, T., Schuenemann, J., Weber, K., and Geisler, N. (1996) *Biochemistry* **35,** 1375–1382
29. Reisdorf, W. C., Jr., and Krimm, S. (1996) *Biochemistry* **35,** 1383–1386

30. Glasoe, P. K., and Long, F. A. (1960) *J. Phys. Chem.* **64,** 188–190
31. Barth, A. (2000) *Prog. Biophys Mol. Biol.* **74,** 141–173
32. Rich, P. R., and Iwaki, M. (2005) *Biophysical and Structural Aspects of Bioenergetics*, p. 314, The Royal Society of Chemistry, Cambridge, UK
33. Iwaki, M., Yakovlev, G., Hirst, J., Osyczka, A., Dutton, P. L., Marshall, D., and Rich, P. R. (2005) *Biochemistry* **44,** 4230–4237
34. Noguchi, T., Inoue, Y., and Tang, X.-S. (1999) *Biochemistry* **38,** 10187–10195
35. Solomon, E. I., Brunold, T. C., Davis, M. I., Kemsley, J. N., Lee, S.-K., Lehnert, N., Neese, F., Skulan, A. J., Yang, Y.-S., and Zhou, J. (2000) *Chem. Rev.* **100,** 235–350
36. Clarkson, A. B., Jr., Bienen, E. J., Pollakis, G., and Grady, R. W. (1989) *J. Biol. Chem.* **264,** 17770–17776
37. Iwaki, M., Giotta, L., Akinsiku, A. O., Schägger, H., Fisher, N., Breton, J., and Rich, P. R. (2003) *Biochemistry* **42,** 11109–11119
38. Breton, J., and Nabedryk, E. (1996) *Biochim. Biophys. Acta* **1275,** 84–90
39. Iwaki, M., and Rich, P. R. (2004) *J. Am. Chem. Soc.* **126,** 2386–2389
40. Rich, P. R. (2004) *Biochim. Biophys. Acta* **1658,** 165–171
41. Koppenhöfer, A., Turner, K. L., Allen, J. W. A., Chapman, S. K., and Ferguson, S. J. (2000) *Biochemistry* **39,** 4243–4249
42. Voevodskaya, N., Narvaez, A.-J., Domkin, V., Torrents, E., Thelander, L., and Gräslund, A. (2006) *Proc. Natl. Acad. Sci. U.S.A.* **103,** 9850–9854
43. Atkin, C. L., Thelander, L., Reichard, P., and Lang, G. (1973) *J. Biol. Chem.* **248,** 7464–7472
44. Albury, M. S., Affourtit, C., Crichton, P. G., and Moore, A. L. (2002) *J. Biol. Chem.* **277,** 1190–1194
45. Moore, A. L., and Albury, M. S. (2008) *Biochem. Soc. Trans.* **36,** 1022–1026
46. Berthomieu, C., and Hienerwadel, R. (2005) *Biochim. Biophys. Acta* **1707,** 51–66
47. Berthomieu, C., Boullais, C., Neumann, J.-M., and Boussac, A. (1998) *Biochim. Biophys. Acta* **1365,** 112–116
48. Berthomieu, C., Hienerwadel, R., Boussac, A., Breton, J., and Diner, B. A. (1998) *Biochemistry* **37,** 10547–10554
49. Walden, S. E., and Wheeler, R. A. (1996) *J. Chem. Soc. Perkin Trans.* **2,** 2663–2672

Acta Crystallographica Section F
Structural Biology and Crystallization Communications
ISSN: 1744-3091
Editors: H. M. Einspahr and M. S. Weiss

Overproduction, purification, crystallization and preliminary X-ray diffraction analysis of *Trypanosoma brucei gambiense* glycerol kinase

Emmanuel Oluwadare Balogun, Daniel Ken Inaoka, Yasutoshi Kido, Tomoo Shiba, Takeshi Nara, Takashi Aoki, Teruki Honma, Akiko Tanaka, Masayuki Inoue, Shigeru Matsuoka, Paul A. M. Michels, Shigeharu Harada and Kiyoshi Kita

Acta Cryst. (2010). F**66**, 304–308

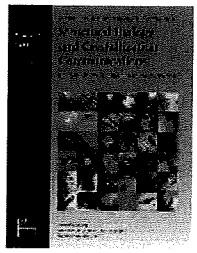

Biochimica et Biophysica Acta 1797 (2010) 443–450

Contents lists available at ScienceDirect

Biochimica et Biophysica Acta

journal homepage: www.elsevier.com/locate/bbabio

Purification and kinetic characterization of recombinant alternative oxidase from *Trypanosoma brucei brucei*

Yasutoshi Kido [a], Kimitoshi Sakamoto [a], Kosuke Nakamura [a], Michiyo Harada [a], Takashi Suzuki [b], Yoshisada Yabu [b], Hiroyuki Saimoto [c], Fumiyuki Yamakura [d], Daijiro Ohmori [d], Anthony Moore [e], Shigeharu Harada [f], Kiyoshi Kita [a,*]

[a] *Department of Biomedical Chemistry, Graduate School of Medicine, The University of Tokyo, Tokyo 113-0033, Japan*
[b] *Department of Molecular Parasitology, Graduate School of Medical Sciences, Nagoya City University, Nagoya 467-8601, Japan*
[c] *Department of Materials Science, Faculty of Engineering, Tottori University, Tottori, Japan*
[d] *Department of Chemistry, School of Medicine, Juntendo University, Tokyo, Japan*
[e] *Biochemistry and Biomedical Sciences, School of Life Sciences, University of Sussex, Falmer, Brighton, UK*
[f] *Department of Applied Biology, Graduate School of Science and Technology, Kyoto Institute of Technology, Kyoto 606-8585, Japan*

ARTICLE INFO

Article history:
Received 24 September 2009
Received in revised form 23 December 2009
Accepted 25 December 2009
Available online 4 January 2010

Keywords:
Alternative oxidase
Membrane-bound diiron protein
Trypanosoma brucei
Ascofuranone
Chemotherapy

ABSTRACT

The trypanosome alternative oxidase (TAO) functions in the African trypanosomes as a cytochrome-independent terminal oxidase, which is essential for their survival in the mammalian host and as it does not exist in the mammalian host is considered to be a promising drug target for the treatment of trypanosomiasis. In the present study, recombinant TAO (rTAO) overexpressed in a haem-deficient *Escherichia coli* strain has been solubilized from *E. coli* membranes and purified to homogeneity in a stable and highly active form. Analysis of bound iron detected by inductively coupled plasma-mass spectrometer (ICP-MS) reveals a stoichiometry of two bound iron atoms per monomer of rTAO. Confirmation that the rTAO was indeed a diiron protein was obtained by EPR analysis which revealed a signal, in the reduced forms of rTAO, with a g-value of 15. The kinetics of ubiquiol-1 oxidation by purified rTAO showed typical Michaelis–Menten kinetics (K_m of 338 μM and V_{max} of 601 μmol/min/mg), whereas ubiquinol-2 oxidation showed unusual substrate inhibition. The specific inhibitor, ascofuranone, inhibited the enzyme in a mixed-type inhibition manner with respect to ubiquinol-1.

1. Introduction

Trypanosoma brucei is a parasite that causes African sleeping sickness in humans and Nagana in livestock and is transmitted by the tsetse fly. There is an urgent need for further development of chemotherapy against African trypanosomiasis since current chemotherapeutic drugs are not entirely satisfactory [1].

Trypanosomal parasites are equipped with a unique energy metabolism, they live as the bloodstream form in the mammalian host and as the procyclic form in the vector. The procyclic form of *T. brucei* fulfills its ATP requirement from a cyanide-sensitive and cytochrome-dependent respiratory chain comparable to that observed in the host mitochondria, whereas in the bloodstream form, trypanosomes use the glycolytic pathway, which is localized in a unique organelle the glycosome, as their major source of ATP [2–5]. Once the parasites invade the mammalian host in the bloodstream form, both its cytochrome-dependent respiratory chain and ATP synthesis by oxidative phosphorylation disappear [2,5]. Instead a cyanide-resistant and cytochrome-independent trypanosomal alternative oxidase (TAO) functions as the sole terminal oxidase to re-oxidize NADH accumulated during glycolysis [5].

TAO is generally considered to be a good target for the anti-trypanosomal drugs because this oxidase is essential for their survival, since it reoxidises cytosolic NADH, and mammalian hosts do not possess this protein [5,6]. Indeed, we found that ascofuranone, isolated from the pathogenic fungus *Ascochyta visiae*, specifically inhibits the quinol oxidase activity of TAO and rapidly kills the parasites [7]. In addition, we have confirmed the chemotherapeutic efficacy of ascofuranone *in vivo* [8,9].

The alternative oxidase (AOX) is a non-protonmotive ubiquinol oxido-reductase catalyzing the 4-electron reduction of dioxygen to water [5,10–12]. Genes encoding AOX have been found in higher

Abbreviations: AOX, alternative oxidase; DM, *n*-dodecyl-β-D-maltopyranoside; EPR, electron paramagnetic resonance; ICP-MS, inductively coupled plasma-mass spectrometer; IPTG, isopropyl, β-D-1-thiogalactoside; k_{cat}, molecular activity; C10E8, octaethylene glycol-monododecylether; OG, *n*-octyl-β-D-glucopyranoside; rTAO, recombinant trypanosome alternative oxidase; SHAM, salycylhydroxamic acid; TAO, trypanosome alternative oxidase; Ubiquinol, reduced form ubiquinone

* Corresponding author. Department of Biomedical Chemistry, Graduate School of Medicine, The University of Tokyo, Hongo, Bunkyo-ku, Tokyo 113-0033, Japan. Tel.: +81 3 5841 3526; fax: +81 3 5841 3444.
E-mail address: kitak@m.u-tokyo.ac.jp (K. Kita).

0005-2728/$ – see front matter © 2009 Elsevier B.V. All rights reserved.
doi:10.1016/j.bbabio.2009.12.021

plants, algae, yeast, slime molds, free-living amoebae, eubacteria and nematodes [13–16]. Moreover, recent bioinformatic searches have broadened the taxonomic distribution of AOX to some members of the animal kingdom [17]. The primary role of AOX in non-thermogenic plants is to regulate cellular redox balance and to protect against reactive oxygen species particularly when the cytochrome pathway is inhibited [18–20]. In addition to this role, many other physiological roles have been described for AOXs in other organisms and these have been discussed in detail elsewhere [13,21]. The ubiquitous occurrence of AOX may suggest that the metabolic flexibility that the alternative pathway confers upon an organism allows it to respond to a wide range of developmental and environmental conditions [22].

Despite universal conservation of the gene and diversified physiology, the molecular features of AOX have not yet been well characterized. Although no high-resolution AOX structure has been determined to date, current structural models predict that it is an integral interfacial membrane protein that interacts with a single leaflet of the lipid bilayer, and contains a non-haem diiron carboxylate active site [23,24]. This model is supported by extensive site-directed mutagenesis studies [18,25–29] and furthermore both EPR and FTIR spectroscopies have confirmed the presence of a binuclear iron center in both the plant and trypanosomal enzymes [30–32].

Further detailed structural and biochemical analyses of AOXs, however, requires further development of purification protocols to produce sufficiently purified and highly active protein to enable crystallization trials and kinetic analyses to proceed. In this paper, we report on the further refinement of our previous protocol through over-expressing rTAO in an *E. coli ΔhemA* mutant (FN102) strain, which lacks quinol oxidase activity of cytochrome *bo* and *bd* complexes [33–35]. Purified rTAO protein is highly active and exhibits an exceptional stability upon storage. The analysis of the prosthetic groups by inductively coupled plasma-mass spectrometer (ICP-MS) and electron paramagnetic resonance (EPR) reveals the presence of two ferric ions stoichiometrically bound per rTAO monomer. To our knowledge this is the first direct confirmation of two ferric irons per AOX. Furthermore we show that purified rTAO is potently inhibited by ascofuranone with mixed function kinetics.

2. Materials and methods

2.1. Preparation of membrane sample

The strain FN102/pTbAO carrying cDNA for *T. b. brucei* TAO [36] was pre-cultured at 37 °C in 100 ml of LB medium containing 10 mg ampicillin, 5 mg kanamycin, and 5 mg 5-aminolevulinic acid for 4–6 h. The pre-cultured cells were aerobically grown at 30 °C in 10 l of S-medium containing 100 g tryptone peptone, 50 g yeast extract, 50 g casamino acid, 104 g K_2HPO_4, 30 g KH_2PO_4, 7.5 g trisodium-citrate·$2H_2O$, 25 g $(NH_4)_2SO_4$, 0.5 g $MgSO_4 \cdot 7H_2O$, 0.25 g $FeSO_4 \cdot 7H_2O$, 0.25 g $FeCl_3$, 0.2%(w/v) glucose, and 1 g carbenicillin. The culture was initiated at O.D.$_{600}$ = 0.01 and expression of rTAO was induced by the addition of isopropyl β-D-1-thiogalactoside (IPTG) (25 μM) at O.D.$_{600}$ = 0.1. Cells were harvested 8–10 h following induction and were resuspended in 50 mM Tris–HCl (pH 7.5) containing 20%(w/w) sucrose, 0.1 mM phenylmethane sulfonyl fluoride (PMSF) and protease inhibitor cocktail (Sigma) and broken by a French Pressure Cell (Ohtake, Tokyo). Unbroken cells were removed by centrifugation at 8000 *g* for 10 min (Hitachi 21G). Inner membranes of FN102/pTbAO were fractionated in high density sucrose after ultracentrifugation at 200,000 *g* for 1 h at 4 °C (Hitachi 85H) (35 ml of supernatant was overlaid over 35 ml of 50 mM Tris–HCl pH 7.5 containing 40%(w/w) sucrose per ultracentrifuge tube). Buoyant inner rich membranes upon 40%(w/w) sucrose layer were fractionated and the inner membrane pellet was separated by further ultracentrifugation at 200,000 *g* for 1 h (HITACHI 85H). The membrane pellet was resuspended in 50 mM Tris–HCl (pH 7.5) containing 20%(w/w) sucrose.

2.2. Solubilization

Membranes were treated with solubilization buffer (6 mg/ml protein in 50 mM Tris–HCl, 1.4%(w/v) *n*-octyl-β-D-glucopyranoside (OG), 200 mM $MgSO_4$, 20%(v/v) glycerol, pH 7.3) at 4 °C and immediately ultracentrifuged at 200,000 *g* for 1 h at 4 °C. The quinol oxidase activities of the samples before centrifugation, as well as that of supernatant and pellet were determined.

2.3. Purification of rTAO

Hybrid batch/column procedure described in the manufacturer's instruction was used as stated below. Ten milliliter of the resin (BD Bioscience, TALON Metal Affinity Resin) was equilibrated in a batch format by 100 ml of equilibration buffer (20 mM Tris–HCl, 1.4%(w/v) OG, 100 mM $MgSO_4$, 20%(v/v) glycerol, pH 7.3). Twenty milliliter of OG extract was mixed with the resin for 20 min at 4 °C. The resin was washed twice with 100 ml of wash buffer (20 mM Tris–HCl, 20 mM imidazole, 0.042%(w/v) *n*-dodecyl-β-D-maltopyranoside (DM), 50 mM $MgSO_4$, 20%(v/v) glycerol pH 7.3) and the resin bound rTAO was transferred to a column for additional washing with 20 ml of second wash buffer (20 mM Tris–HCl, 165 mM imidazole, 0.042%(w/v) DM, 50 mM $MgSO_4$, 20%(v/v) glycerol pH 7.3; flow rate 1 ml/min) and protein elution. Finally, rTAO was eluted with elution buffer (20 mM Tris–HCl, 200 mM imidazole, 0.042%(w/v) DM, 50 mM $MgSO_4$, 60 mM NaCl, 20%(v/v) glycerol pH 7.3; flow rate 1 ml/min). Fractions (4 ml each) were collected.

2.4. Quantitative analysis of metals and EPR spectroscopy

Three independent preparations of rTAO were analyzed (details in Section 3). Each sample solution containing 0.1 g of rTAO was added to 1 ml of nitric acid and 7 ml of water. Organic compounds were hydrolyzed by microwave-assisted protein digestion system (Ethos Pro, Milestone General). Fe, Mn, Cu, Zn and Co in each sample were quantified by inductively coupled plasma-mass spectrometer (ICP-MS, ELAN DRC PerkinElmer Japan). Analysis was performed by the Sumika Chemical Analysis Center (Osaka, Japan). Protein concentration was determined by the Lowry method.

EPR spectra were recorded on a JEOL X-band JES-FA300 spectrometer equipped with an ES-CT470 Heli-Tran cryostat system and a Scientific Instruments digital temperature indicator/controller model 9700a. For EPR analysis of rTAO, 13 mg/ml purified rTAO was frozen in EPR tubes in liquid nitrogen. The purified rTAO was reduced by 2 mM dithionite and 1 mM phenazine methosulfate prior to freezing.

2.5. Ubiquinol oxidase assay

Ubiquinol oxidase activity was measured by recording the absorbance change of ubiquinol-1 at 278 nm (Shimadzu spectrophotometer UV-3000). Reactions were started by the addition of ubiquinol-1 (final concentration 150 μM, $\varepsilon_{278} = 15{,}000\ M^{-1}\ cm^{-1}$) after 2 min preincubation at 25 °C in the presence of rTAO and 50 mM Tris–HCl (pH 7.4). For the enzyme kinetics of purified rTAO, the reaction was initiated by the addition of ubiquinol-1 after 2 min preincubation at 25 °C in the presence of rTAO and 50 mM Tris–HCl (pH 7.4) containing 0.05%(w/v) octaethylene glycol-monododecylether detergent (C10E8).

2.6. Chemicals

All chemicals were biochemistry grade. Ubiquinone-1 and protease inhibitor cocktail were purchased from Sigma-Aldrich. The other detergents were purchased from Dojin Chemicals (Tokyo, Japan).

3. Results

3.1. Purification of fully active TAO

Although we previously established a protocol for the overproduction of rTAO in *E. coli* FN102 (*ΔhemA*) lacking cytochrome *bo* and *bd* complexes of the bacteria, the yield of the active enzyme was too low to analyze its prosthetic group [36]. Such a preparation also hampered the determination of kinetic parameters of rTAO such as its molecular activity. Therefore, conditions for the expression of rTAO and purification protocols were optimized to obtain large quantities of active and stable rTAO to enable such determinations. Three factors were critical to obtain large amounts of active rTAO, namely, growth time of the culture prior to addition of IPTG, absolute concentration of IPTG, and the use of purified inner membranes as the starting material.

After extensive screening of detergents and additives to establish the procedure for efficient extraction of active rTAO from the inner membranes, we found that *n*-octyl-*β*-D-glucopyranoside (OG) specifically solubilized rTAO as shown in Table 1 (specific activity increased from 23.3 to 63.2 μmol/min/mg after solubilization). Approximately 60% of the membrane quinol oxidase activity was recovered with 1.4%(w/v) OG in the extract (Sup. Fig. 1). Thus, recovery of the activity was significantly higher than that of previously reported digitonin extraction (17%) [36]. Following solubilization, it was possible to maintain enzymatic activity for at least 1 month at 20 °C.

Since rTAO was fused with N-terminal histidine tag, solubilized rTAO was purified by cobalt affinity chromatography. Although the enzyme solubilized by OG was bound to the cobalt affinity resin in the presence of OG, it was not possible to elute bound rTAO from the resin with buffer containing OG. Interestingly, however, we found that 100% of the rTAO activity could be recovered from the column when OG in the washing and elution buffers was exchanged with *n*-dodecyl-*β*-D-maltopyranoside (DM). In the final step, purified rTAO was obtained by a two-step elution with 165 mM and 200 mM imidazole, which resulted in a very efficient purification of active rTAO in the presence of DM. A typical elution profile of quinol oxidase activity with increasing imidazole concentration is shown in Sup. Fig. 1B. Purified rTAO, with a molecular mass of 34 kDa, was estimated to be 95% pure by SDS-PAGE (Fig. 1A, lane 5). In addition to the 34 kDa band, it is apparent that other bands are also present including two with a smaller size than rTAO and one band with an approximate molecular mass of 74 kDa. Since all of these bands were recognized in Western blot using a monoclonal antibody against TAO (Fig. 1B), the smaller protein bands possibly represent proteolytic breakdown products whilst the 74 kDa band most likely represents the dimeric form of rTAO. The specific activity of purified rTAO was more than 200 μmol/min/mg protein when 150 μM of ubiquinol-1 was used as a substrate, which had a five-fold higher activity than that of the previously purified rTAO (approximately 40 μmol/min/mg) [36]. Quinol oxidase activity of purified rTAO was insensitive to 5 mM KCN but was completely inhibited by 10 nM ascofuranone. A greater than 35-fold increase in purification was achieved using the techniques described above, and 13.2% of the total activity was recovered from the lysate of FN102/pTAO cells as summarized in Table 1. Such procedures resulted in approximately 10 mg of highly purified rTAO from a 10 l culture.

Table 1
Purification of rTAO.

Fractions	Total activity (μmol/min)	Protein (mg)	Specific activity (μmol/min/mg)	Recovery (%)
E. coli lysate	14100	2410	5.85	100
Inner membrane	3500	150	23.3	24.8
OG extract	2400	37.9	63.2	17.0
Co-column	1860	8.95	207	13.2

The activities listed here were measured using 150 μM of ubiquinol-1. Fractions (eluate numbers 6–13 in Supplemental Fig. 1B) were collected as purified rTAO after co-column.

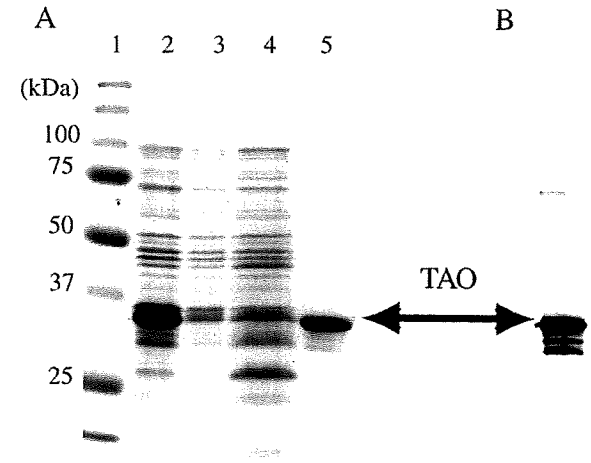

Fig. 1. SDS-PAGE and Western blotting of rTAO in purification steps. A: CBB-staining 12.5% SDS-PAGE of each fraction from the cobalt column chromatography. Lane 1, marker; lanes 2 and 3, each 5 ml of OG extract and flow through fraction; lane 4, 500 ml of wash fraction; and lane 5, 60 ml of eluted fraction collected from fractions 6–12. Loading samples on lanes 2 to 5 were precipitated with acetone. B: Western blot of purified rTAO. The same sample to lane 5 in panel B was electrophoresed on 12.5% polyacrylamide gel. Monoclonal antibodies were used against highly purified rTAO obtained by a nickel column in the presence of guanidine. Epitope recognized by this antibody is the C-terminal domain of the enzyme. The arrow indicates rTAO with an apparent molecular mass of 34 kDa.

3.2. Iron content in purified TAO

Since a highly active and stable purified rTAO could be obtained by the protocol described above, the metal content of purified rTAO was measured by ICP-MS. On the basis that TAO has a diiron center as previously proposed [23,24], then two equivalents of iron should be detected per monomer of rTAO. To this end we analyzed the iron content of purified native rTAO, inactive rTAO, denatured rTAO, and iron within the buffer eluted from the cobalt-column. Purified native rTAOs derived from three independent *E. coli* cultures were precipitated by PEG 3350 and resuspended in the elution buffer at three different concentrations as shown in Sup. Table 1. To prepare inactive rTAO, precipitated rTAO was resuspended in 50 mM Tris–HCl pH 7.4, which resulted in complete loss of enzyme activity. Denatured rTAO was prepared by resuspending the precipitant in elution buffer containing 6 M guanidine–HCl and 0.3 M EDTA. Metal contents in these preparations were 9000 ng/ml, 2900 ng/ml and 1800 ng/ml of Fe respectively for the native rTAO (3.71, 1.19 and 0.80 mg/ml), 230 ng/ml, 100 ng/ml and 28 ng/ml of Fe for inactive rTAO, denatured rTAO and the elution buffer, respectively (Sup. Table 1). From these results, the stoichiometry of bound iron per rTAO monomer can be deduced as indicated below, based on the following parameters namely, a molecular mass of rTAO of 39,391 Da (including the 6×histidine tag), purity of 95% based on SDS-PAGE gels, and the atomic weight of Fe being 55.85. Thus the ratio of iron atoms per rTAO is 1.76 for native rTAO and 0.2 and 0.08 in inactive rTAO and denatured rTAO, respectively (Table 2). This data indicates that one monomer of TAO possesses two atoms of iron which are released during inactivation or denaturation of the enzyme. To our knowledge, this is the first direct measurement of iron in purified AOX and the stoichiometry is consistent with the active site of AOX being a diiron carboxylate-center.

Other metals including Mn, Cu and Zn were also analyzed (Sup. Table 1). In all cases, these metals were below their detection limit (10 ng/ml sample solution) or background level. Although cobalt was

Table 2
Ratio of metals to purified rTAO.

	Fe/rTAO	Zn/rTAO	Mn/rTAO	Cu/rTAO
	Mean ± S.D.			
Native rTAO	1.76 ± 0.077	0.03 ± 0.013	N.D.[a]	N.D.
Inactive rTAO	0.22[b]	N.D.	N.D.	N.D.
Denatured rTAO	0.08[b]	N.D.	N.D.	N.D.

Stoichiometric ratio of metals to one molecular TAO was calculated using data in Supplemental Table 1.
[a] N.D. represents Not Detected (below 0.01).
[b] The value is an average of two independent experiments.

detected in purified rTAO, its concentration was comparable to that of cobalt in the elution buffer derived from the resin (data not shown). Similarly although 130 ng/ml, 66 ng/ml and 61 ng/ml of Zn were detected in native rTAO, these amounts of Zn were not commensurate with that of the enzyme stoichiometry. The detected Zn might be derived from the Zn-substituted form of rTAO, which was suggested to be possible from structural analysis [37]. In addition, at least 90% of the purified rTAO retained its prosthetic group in its active form.

In addition to measuring the stoichiometry of iron in purified rTAO, EPR analysis of purified rTAO was also performed in order to confirm that purified rTAO was indeed a diiron carboxylate protein and whether the detected iron originated from a diiron binding center. As shown in Fig. 2, a low field EPR signal at approximately $g = 15$ in the perpendicular EPR mode was observed with the reduced form of rTAO when the enzyme was reduced by 2 mM of dithionite and 1 mM of phenazine methosulfate (PMS), although the intensity of the signal was low. Importantly the signal disappeared in the oxidized form of rTAO. This low field EPR signal is characteristic for diiron proteins and is ascribed to an exchange-coupled high spin ferrous iron [38]. Although this signal is not normally observed in the perpendicular mode, it can be detected under certain conditions as outlined in this report [39]. The effective g-value of 15 observed in the perpendicular mode is slightly lower than the value of 16 previously observed by us [31] but this is probably due to the fact that parallel-mode EPR spectroscopy is a much more sensitive probe than the perpendicular mode. Nevertheless the finding of a low field signal when the purified enzyme is reduced is further confirmation that the purified rTAO we report here is indeed a diiron carboxylate protein. It should be noted however that we were unable to observe the $g = 15$ signal when the enzyme was reduced by more physiological reductants such as ubiquinol-1 the reasons for which are, at present, unclear.

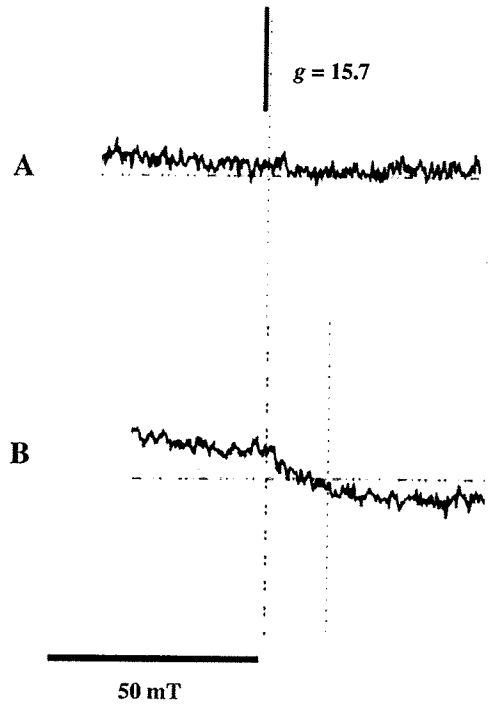

Fig. 2. EPR spectra of rTAO. A: Oxidized form of rTAO (360 μM). B: Reduced form of rTAO (360 μM), which was treated by 2 mM of dithionite and 1 mM phenazine methosulfate for 30 min on ice. Instrument parameters: microwave frequency, 9.02 GHz; microwave power, 1 mW; modulation frequency, 100 kHz; modulation amplitude, 0.6 mT; and temperature of 5 K.

3.3. Kinetic properties of purified TAO

Kinetic analysis of purified rTAO (or AOX) using ubiquinone analogs has previously proved difficult because: 1) the enzyme, following solubilization, was extremely unstable, 2) the natural substrate of trypanosome AOX is ubiquinol-9 [4], which is too hydrophobic to use as the substrate in the assay and 3) the enzymatic activity was not saturated at the maximum concentration of ubiquinol-1 (approximately 300 μM). Since we have purified rTAO in a fully active form and confirmed the stoichiometric presence of the diiron center, the purified rTAO was well-suited to a kinetic analysis.

As noted in our earlier study [36] and in AOXs from other organisms [40] non Michaelis–Menten kinetics is observed when ubiquinol-1 is used as a substrate. Hoefnagel et al. [40], however, observed that the addition of a specific detergent (0.025% EDT-20) during the assay increased the activity by 3- to 4-fold close to saturation. Although the addition of 0.025%(w/v) of EDT-20 equally enhanced the activity of purified rTAO by approximately 2-fold, it did have a deleterious effect upon the long term stability of the enzyme (Sup. Fig. 2).

In an attempt to overcome this problem, various detergents were therefore screened to determine if they could enhance activity without affecting enzyme stability. When the effect of the detergents on enzyme activity was evaluated by monitoring the activity of rTAO in the presence of detergent (Sup. Fig. 3), most activity was retained in the presence of 0.05%(w/v) of C10E8 (Sup. Fig. 4A). Light scattering at 400 nm confirmed that at least 600 μM of ubiquinol-1 was soluble in the assay system (Sup. Fig. 4B). The kinetics of ubiquinol-1 oxidation by purified rTAO in the presence of 0.05%(w/v) of C10E8 showed typical Michaelis–Menten kinetics (Fig. 3, K_m of 338 ± 23.2 μM and V_{max} of 601 ± 27.0 μmol/min/mg). In contrast, activity was linearly dependent upon substrate concentration in the absence of detergent indicating unsaturation in agreement with previous studies [36,40] (Fig. 4). Enzymatic analysis was performed with a wide range of

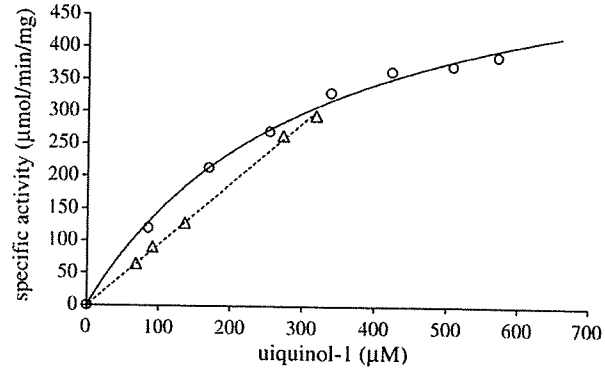

Fig. 3. Kinetics of ubiquinol-1 oxidation by purified rTAO. S–V plot of ubiquinol oxidase activity is shown using 75 ng of purified rTAO in 50 mM Tris–HCl (pH 7.4) and ubiquinol-1 (80–580 μM) with (○) and without (△) 0.05%(w/v) C10E8 at 25 °C. The solid line indicates the fitted Michaelis–Menten kinetics with the detergent (K_m of 338 ± 23.2 μM and V_{max} of 601 ± 27.0 μmol/min/mg), whereas the dashed line indicates the linear relationship between the substrate concentration and the activity without the detergent.

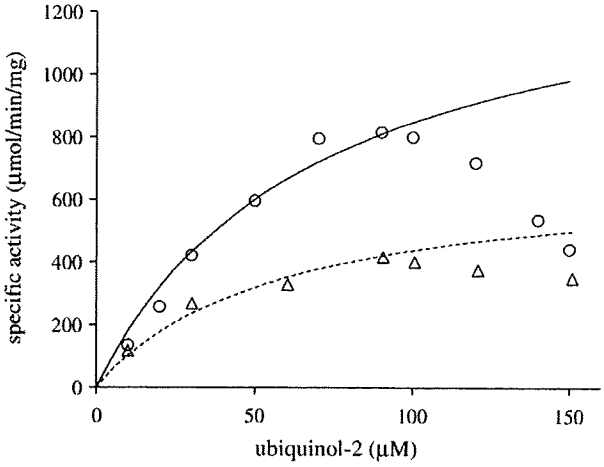

Fig. 4. Kinetics of ubiquinol-2 oxidation by purified rTAO. S–V plot of ubiquinol oxidase activity is shown using 75 ng of purified rTAO in 50 mM Tris–HCl (pH 7.4) and ubiquinol-2 (10–150 μM) with (△) 0.05%(w/v) C10E8 and with (○) 0.025%(w/v) EDT-20 at 25 °C. The solid line indicates the fitted Michaelis–Menten kinetics in the concentration range below 90 μM of ubiquinol-2 with 0.025%(w/v) EDT-20, whereas the dashed line does with 0.05%(w/v) C10E8 (K_m of 71 ± 1.2 μM and V_{max} of 1,460 ± 53.2 μmol/min/mg with 0.025%(w/v) EDT-20, whereas K_m of 57 ± 8.5 μM and V_{max} of 691 ± 28.0 μmol/min/mg with 0.05%(w/v) C10E8).

substrate concentrations (80–570 μM), which corresponded to 0.4 K_m–1.7 K_m.

To investigate whether the length of the side chain of the substrate affected the kinetic properties of rTAO, a kinetic analysis using ubiquinol-2 in the presence of EDT-20 and C10E8 (Fig. 4) was performed. Fig. 4 indicates that during the oxidation of ubiquinol-2, enzyme activity decreased above 100 μM substrate even in buffers containing either detergent. Although kinetic parameters using ubiquinol-2 could not be obtained due to substrate inhibition, S–V plots in the concentration range below 90 μM of ubiquinol-2 could be used to qualitatively analyze the effects of side chain on enzyme activity. Calculated values from such plots revealed that in the presence of 0.025%(w/v) EDT-20 the K_m (ubiquinol-2) was 71 ± 1.2 μM and V_{max} = 1460 ± 53.2 μmol/min/mg whereas with, 0.05%(w/v) C10E8 the K_m was 57 ± 8.5 μM and V_{max} = 691 ± 28.0 μmol/min/mg.

Ascofuranone is a highly specific and potent inhibitor of TAO [7] and it was therefore of importance to determine its inhibitory effect on ubiquinol-1 oxidation by purified rTAO in the presence of 0.05%(w/v) of C10E8 (Sup. Fig. 5A). From the data presented in Sup. Fig. 5A the apparent kinetic parameters of ubiquinol-1 oxidation in the presence of 0.5 nM and 2 nM of ascofuranone were estimated to be respectively $K_m^{0.5\,nM}$ = 368 ± 6.4 μM; $V_{max}^{0.5\,nM}$ = 490 ± 22.4 μmol/min/mg and $K_m^{2\,nM}$ = 492 ± 7.2 μM; and $V_{max}^{2\,nM}$ = 309 ± 60.5 μmol/min/mg. The increased K_m and decreased V_{max} values (Sup. Fig. 5B) indicate that ascofuranone inhibits purified rTAO in a mixed-type non-competitive manner with respect to ubiquinol-1.

4. Discussion

The overall goal of the present study was to obtain a highly pure and stable rTAO protein with maximum specific activity which could be used to investigate the kinetic properties of the enzyme. The quality of the purified rTAO obtained in this study has resulted in three important aspects with respect to the structure of AOX namely, the first direct evidence of stoichiometrically bound iron within the diiron center of rTAO, secondly reliable measurements of kinetic parameters and thirdly that a sample of sufficient purity and yield could be produced that has resulted in the formation of crystals [41].

4.1. Overexpression and purification of rTAO

The difficulties in isolating stable AOXs in an active form have hampered the biochemical and structural analyses of the enzyme including identification of its prosthetic groups, tertiary structural analysis and the definition of enzyme kinetic parameters. The present study reports on the overexpression and purification of active rTAO, which has enabled us to study biochemical and protein chemistry properties of this enzyme. The protocol described in this paper results in the purification of large amounts of stable rTAO with high specific activity. Two factors appeared critical to functionally express highly active rTAO. Firstly, the optimization of culture conditions, including culture duration and IPTG concentration, was crucial for the successful overexpression of rTAO with high specific activity. Secondly, activity was maximized when rTAO was purified from *E. coli* inner membranes—activity decreased substantially when it was isolated from an unpurified membrane fraction. Additionally, changing the detergent from OG to DM following solubilization, also appeared important to maximize yield and activity. Purified rTAO produced in this manner retained complete activity for more than 6 months at 4 °C and for more than 1 month at 20 °C. Furthermore, we have also been able to purify *Sauromattum guttatum* rAOX by this procedure showing the universality of the purification protocol (Elliott, C.E., Kido, Y., Kita, K. and Moore, A.L. unpublished observations).

It is anticipated that highly purified and active AOX will open a new direction with respect to the investigation of the structure and reaction mechanisms of AOXs and contribute to further progress on the study of this novel terminal oxidase. Indeed we recently took advantage of the exceptional stability and purity of the rTAO by performing the first FTIR spectroscopic investigation of any diiron protein [32]. Stepwise reduction of the fully oxidized resting state of rTAO revealed two distinct IR redox difference spectra. The first of these, "signal 1", contained clear features that could be assigned to protonation of at least one carboxylate group, further perturbations of carboxylic and histidine residues, bound ubiquinone and a negative band that might arise from a radical in the fully oxidized protein. A second IR redox difference spectrum, "signal 2", appeared more slowly (within approximately 1 h) once signal 1 had been reduced and is quite distinct from the components which comprise signal 1. The exact identity of the components which result in signal 2 await further investigations. Such a study has not previously been possible with AOX preparations because of protein instability at room temperature.

4.2. Prosthetic group analysis

Prosthetic group analysis summarized in Table 2 revealed that in highly stable and purified rTAO there are two equivalents of iron per rTAO monomer with no other metals, including Cu, Mn and Zn, being detected. EPR spectroscopy confirms that the irons are part of a diiron center since an EPR signal at $g = 15$ could be detected (Fig. 2) when rTAO is reduced by dithionite in the presence of PMS. The fact that this signal can be detected in all AOXs examined to date suggests that the signal is a characteristic signature of AOXs [30,31] and in agreement with mutational analyses [18,25–29] is further confirmation that TAO, similar to AOXs in other organisms, is a diiron carboxylate protein. Furthermore the data summarized in Table 2 revealed that when the protein was either inactivated or denatured iron was released indicating it is essential for TAO activity. Moreover, this data has established biochemically the validity of predicting the presence of a diiron center from amino acid sequence data, not only in AOX but also in other membrane-bound diiron carboxylate proteins including 5-demethoxyquinone hydroxylase (CLK-1/Coq7) (which also has the diiron binding motif EXXH). It is of interest to note that both AOX and CLK-1/Coq7 utilize ubiquinol as substrate and both are involved in respiration [42–44].

4.3. Kinetic analysis

The inclusion of C10E8 in the assay was found to be critical for the kinetic analysis of TAO and the evaluation of inhibitors. In Table 3, we have calculated fundamental kinetic parameters of TAO and compared them to those of *E. coli* cytochrome *bo* oxidase complex and *S. cerevisiae* ubiquinol–cytochrome *c* reductase [45]. These kinetic constants provide a molecular rationale on how the alternative pathway can effectively compete with other terminal oxidases, although caution must be exercised in the interpretation of this data as it is derived from experiments performed under non-physiological conditions and substrates. Nevertheless Table 3 indicates that TAO has a calculated k_{cat} of $415 \pm 19\ s^{-1}$ (on the basis that the purity of rTAO is 95%), which is slightly higher than that of the cytochrome *bo* oxidase complex ($313\ s^{-1}$), yeast ubiquinol–cytochrome *c* reductase ($153\ s^{-1}$) and previous values reported for the plant AOX ($186\ s^{-1}$), but considerably less than that calculated for cytochrome *c* oxidase ($770\ s^{-1}$) [45–48]. Taking into account that the value of the specificity constant (k_{cat}/K_m) of enzymatic reactions is known to be less than $10^9\ M^{-1}\ s^{-1}$ (from the perspective of diffusion limited access of substrates [49]), it is apparent from Table 3 that both cytochrome *bo* oxidase and TAO have quite high and comparable catalytic activities. These values suggest that the activation energy of both quinol oxidase reactions are similar and furthermore that the quinol oxidase activity of TAO is thermodynamically "alternative" to that of the cytochrome *bo* complex. In contrast however, TAO does not appear to compete effectively with the bc_1 complex in terms of specificity constant and, if the plant AOX possesses a similar specificity constant to that of TAO, it would suggest that plant alternative oxidase activity would be severely curtailed unless the conventional respiratory chain is limited either through inhibition (which appears to be the case under 'stressed conditions') or through down regulation as appears to be the case in thermogenic tissues [12,50,51].

Interestingly ubiquinol-2 oxidation by rTAO showed substrate inhibition at concentrations above 100 μM in a manner similar to that observed when the heterodimeric terminal ubiquinol oxidase of *E. coli*, cytochrome *bd* oxidized ubiquinol-2 as substrate [52]. A lower K_m value of ubiquinol-2 than that of ubiquinol-1 might be related not only to its hydrophobicity but also could be a function of the isoprenoid chain. The peculiar kinetics of ubiquinol-2 might be attributed to the following two points; 1) competition for the ubiquinol-2 oxidation site between the substrate and the product, and 2) the presence of inactive intermediates of the enzyme related to the precise catalytic mechanism.

Kinetic analysis of the mechanism of inhibition by the specific TAO inhibitor ascofuranone (Sup. Fig. 5) indicates that it is a mixed-type inhibitor with respect to ubiquinol-1. The discrepancy between the mixed inhibition observed in this report and competitive inhibition as reported in our previous study [36] might be due to the different assay conditions used in the experiments described in this paper. In the previous study, the kinetic parameters were based on apparent values because enzymatic activity was calculated without detergents and hence only low ranges of ubiquinol-1 concentrations (0.01 K_m–0.3 K_m) could be used. In contrast, the kinetic parameters reported in the current study were determined with much higher reliability since in the presence of C10E8, a much wider range of ubiquinol-1 (0.4 K_m–1.7 K_m) could be used.

Table 3
Kinetic parameters of quinol oxidases (with respect to ubiquinol-1).

	K_m (μM)	V_{max} (μmol/min/mg protein)	k_{cat} (s^{-1})	k_{cat}/K_m ($\mu M^{-1} s^{-1}$)
TAO[a]	338 ± 23.2	601 ± 27.0	415 ± 19	1.2
Cyt *bo* oxidase[b]	61	–	313	5.2
Ubiquinol-cyt *c* reductase[c]	13	–	220	16.9

The k_{cat} value of cytochrome *c* oxidase is $k_{cat} = 770\ (s^{-1})$ [46].
All the k_{cat} values listed here were obtained by dividing the V_{max} by the concentration of the enzymes (mol/mg protein).
[a] This study.
[b] *E. coli* cytochrome *bo* oxidase as in Sakamoto et al. [47].
[c] Ubiquinol–cytochrome *c* reductase from bovine heart as in Fato et al. [45].

4.4. Unique feature of AOX

AOX is found in various organisms and recent genome database searches have also identified AOX in different phyla of the Animalia kingdom (Mollusca, Nematoda and Chordata) [17]. It has been suggested that since AOX is absent from mammalian tissues TAO could be a chemotherapeutic target, since it functions in the bloodstream form of *T. brucei* as the only terminal oxidase and hence is essential for the survival of trypanosomes [5,6]. As an AOX protein has also been identified in *Cryptosporidium parvum* [53,54], which causes diarrheal disease cryptosporidiosis, and the recombinant *C. parvum* AOX is also sensitive to ascofuranone and as a result suggests that not only could AOX be a potential drug target in a number of parasites but furthermore ascofuranone could be used to treat a number of infections since this compound shows potent, broad-spectrum antimicrobial activity [53].

In addition to this clinical application, there is considerable interest in the unique characteristics of the enzyme since the functions and properties of TAO are clearly distinct from those of other bacterial quinol oxidases. TAO is a cytochrome-independent and cyanide-insensitive quinol oxidase, whereas cytochrome *bo* and *bd* complexes are cytochrome-dependent and cyanide-sensitive quinol oxidases [34,35]. Furthermore, TAO has various other physiological roles in *T. brucei*; the cytochrome and alternative pathways are both active and functional in the procyclic forms [55] in addition to the bloodstream form, thereby possibly providing metabolic flexibility under changing environmental conditions. TAO activity also appears to regulate the expression of one of the major surface coat proteins, GPEET, in the procyclic form [56], and in addition may regulate the observed programmed cell death-like phenomena in the bloodstream forms [57].

5. Conclusions

The primary aim of our research on TAO is to elucidate the interaction between the enzyme and its substrate or inhibitor, which hopefully could act as a structural guide for ongoing drug development. In addition to the knowledge obtained from this study, further studies on the inhibitory kinetics and structure–activity relationship of ascofuranone derivatives, along with mutational analyses of TAO [27,29] and X-ray structure analysis will undoubtedly have considerable implications with respect to our understanding of how the enzyme interacts with its substrate and inhibitors. A three-dimensional structure of TAO with and without ascofuranone should also shed light on the inhibitory mechanism of this potent drug, which according to this study occurs via a mixed-type inhibition. Such further insights about the interaction between ascofuranone and the enzyme will hopefully lead to a more rational design of more potent and safe anti-trypanosomal drugs.

Acknowledgements

This work was supported in part by Grant-in-aid for Young Scientists (B) 21790402 (to YK), Grant-in-Aid for Scientific Research (C) 21590467 (to YY), Creative Scientific Research Grant 18GS0314 (to KK), Grant-in-aid for Scientific Research on Priority Areas 18073004 (to KK) from the Japanese Society for the Promotion of Science, and Targeted Proteins Research Program (to KK) from the

Japanese Ministry of Education, Science, Culture, Sports and Technology (MEXT) and a grant for research to promote the development of anti-AIDS pharmaceuticals from the Japan Health Sciences Foundation (to KK). ALM gratefully acknowledges BBSRC for financial support and with KK the Prime Ministers Initiative 2 (Connect) fund for collaborative twinning.

Appendix A. Supplementary data

Supplementary data associated with this article can be found, in the online version, at doi:10.1016/j.bbabio.2009.12.021.

References

[1] WHO, Control and surveillance of African trypanosomiasis, Report of a WHO Expert Committee, World Health Organ Tech Rep Ser, vol. 881, 1998, pp. 1–114, I–VI.
[2] C.E. Clayton, P. Michels, Metabolic compartmentation in African trypanosomes, Parasitol. Today 12 (1996) 465–471.
[3] F.R. Opperdoes, P. Borst, S. Bakker, W. Leene, Localization of glycerol-3-phosphate oxidase in the mitochondrion and particulate NAD+-linked glycerol-3-phosphate dehydrogenase in the microbodies of the bloodstream form to *Trypanosoma brucei*, Eur. J. Biochem. 76 (1977) 29–39.
[4] A.B. Clarkson Jr., E.J. Bienen, G. Pollakis, R.W. Grady, Respiration of bloodstream forms of the parasite *Trypanosoma brucei brucei* is dependent on a plant-like alternative oxidase, J. Biol. Chem. 264 (1989) 17770–17776.
[5] M. Chaudhuri, R.D. Ott, G.C. Hill, Trypanosome alternative oxidase: from molecule to function, Trends Parasitol. 22 (2006) 484–491.
[6] C. Nihei, Y. Fukai, K. Kita, Trypanosome alternative oxidase as a target of chemotherapy, Biochim. Biophys. Acta 1587 (2002) 234–239.
[7] N. Minagawa, Y. Yabu, K. Kita, K. Nagai, N. Ohta, K. Meguro, S. Sakajo, A. Yoshimoto, An antibiotic, ascofuranone, specifically inhibits respiration and in vitro growth of long slender bloodstream forms of *Trypanosoma brucei brucei*, Mol. Biochem. Parasitol. 84 (1997) 271–280.
[8] Y. Yabu, A. Yoshida, T. Suzuki, C. Nihei, K. Kawai, N. Minagawa, T. Hosokawa, K. Nagai, K. Kita, N. Ohta, The efficacy of ascofuranone in a consecutive treatment on *Trypanosoma brucei brucei* in mice, Parasitol. Int. 52 (2003) 155–164.
[9] Y. Yabu, T. Suzuki, C. Nihei, N. Minagawa, T. Hosokawa, K. Nagai, K. Kita, N. Ohta, Chemotherapeutic efficacy of ascofuranone in *Trypanosoma vivax*-infected mice without glycerol, Parasitol. Int. 55 (2006) 39–43.
[10] M. Chaudhuri, W. Ajayi, S. Temple, G.C. Hill, Identification and partial purification of a stage-specific 33 kDa mitochondrial protein as the alternative oxidase of the *Trypanosoma brucei brucei* bloodstream trypomastigotes, J. Eukaryot. Microbiol. 42 (1995) 467–472.
[11] A.L. Moore, J.N. Siedow, The regulation and nature of the cyanide-resistant alternative oxidase of plant mitochondria, Biochim. Biophys. Acta 1059 (1991) 121–140.
[12] A.L. Moore, M.S. Albury, Further insights into the structure of the alternative oxidase: from plants to parasites, Biochem. Soc. Trans. 36 (2008) 1022–1026.
[13] J.N. Siedow, A.L. Umbach, The mitochondrial cyanide-resistant oxidase: structural conservation amid regulatory diversity, Biochim. Biophys. Acta 1459 (2000) 432–439.
[14] T. Joseph-Horne, D.W. Hollomon, P.M. Wood, Fungal respiration: a fusion of standard and alternative components, Biochim. Biophys. Acta 1504 (2001) 179–195.
[15] A. McDonald, G. Vanlerberghe, Branched mitochondrial electron transport in the Animalia: presence of alternative oxidase in several animal phyla, IUBMB Life 56 (2004) 333–341.
[16] A.E. McDonald, G.C. Vanlerberghe, Alternative oxidase and plastoquinol terminal oxidase in marine prokaryotes of the Sargasso Sea, Gene 349 (2005) 15–24.
[17] A.E. McDonald, G.C. Vanlerberghe, J.F. Staples, Alternative oxidase in animals: unique characteristics and taxonomic distribution, J. Exp. Biol. 212 (2009) 2627–2634.
[18] D.A. Berthold, M.E. Andersson, P. Nordlund, New insight into the structure and function of the alternative oxidase, Biochim. Biophys. Acta 1460 (2000) 241–254.
[19] C. Affourtit, M.S. Albury, P.G. Crichton, A.L. Moore, Exploring the molecular nature of alternative oxidase regulation and catalysis, FEBS Lett. 510 (2002) 121–126.
[20] D.P. Maxwell, Y. Wang, L. McIntosh, The alternative oxidase lowers mitochondrial reactive oxygen production in plant cells, Proc. Natl. Acad. Sci. U. S. A. 96 (1999) 8271–8276.
[21] A.L. Moore, M.S. Albury, P.G. Crichton, C. Affourtit, Function of the alternative oxidase: is it still a scavenger? Trends Plant Sci. 7 (2002) 478–481.
[22] S. Mackenzie, L. McIntosh, Higher plant mitochondria, Plant Cell 11 (1999) 571–586.
[23] J.N. Siedow, A.L. Umbach, A.L. Moore, The active site of the cyanide-resistant oxidase from plant mitochondria contains a binuclear iron center, FEBS Lett. 362 (1995) 10–14.
[24] M.E. Andersson, P. Nordlund, A revised model of the active site of alternative oxidase, FEBS Lett. 449 (1999) 17–22.
[25] M.S. Albury, C. Affourtit, A.L. Moore, A highly conserved glutamate residue (Glu-270) is essential for plant alternative oxidase activity, J. Biol. Chem. 273 (1998) 30301–30305.
[26] M. Chaudhuri, W. Ajayi, G.C. Hill, Biochemical and molecular properties of the *Trypanosoma brucei* alternative oxidase, Mol. Biochem. Parasitol. 95 (1998) 53–68.
[27] W.U. Ajayi, M. Chaudhuri, G.C. Hill, Site-directed mutagenesis reveals the essentiality of the conserved residues in the putative diiron active site of the trypanosome alternative oxidase, J. Biol. Chem. 277 (2002) 8187–8193.
[28] M.S. Albury, C. Affourtit, P.G. Crichton, A.L. Moore, Structure of the plant alternative oxidase. Site-directed mutagenesis provides new information on the active site and membrane topology, J. Biol. Chem. 277 (2002) 1190–1194.
[29] K. Nakamura, K. Sakamoto, Y. Kido, Y. Fujimoto, T. Suzuki, M. Suzuki, Y. Yabu, N. Ohta, A. Tsuda, M. Onuma, K. Kita, Mutational analysis of the *Trypanosoma vivax* alternative oxidase: the $E(X)_6Y$ motif is conserved in both mitochondrial alternative oxidase and plastid terminal oxidase and is indispensable for enzyme activity, Biochem. Biophys. Res. Commun. 334 (2005) 593–600.
[30] D.A. Berthold, N. Voevodskaya, P. Stenmark, A. Graslund, P. Nordlund, EPR studies of the mitochondrial alternative oxidase. Evidence for a diiron carboxylate center, J. Biol. Chem. 277 (2002) 43608–43614.
[31] A.L. Moore, J.E. Carre, C. Affourtit, M.S. Albury, P.G. Crichton, K. Kita, P. Heathcote, Compelling EPR evidence that the alternative oxidase is a diiron carboxylate protein, Biochim. Biophys. Acta 1777 (2008) 327–330.
[32] A. Maréchal, Y. Kido, K. Kita, A.L. Moore, P.R. Rich, Identification of three redox states of recombinant *Trypanosoma brucei* alternative oxidase by FTIR spectroscopy and electrochemistry, J. Biol. Chem. 284 (2009) 31827–31833.
[33] Y. Fukai, H. Amino, H. Hirawake, Y. Yabu, N. Ohta, N. Minagawa, S. Sakajo, A. Yoshimoto, K. Nagai, S. Takamiya, S. Kojima, K. Kita, Functional expression of the ascofuranone-sensitive *Trypanosoma brucei brucei* alternative oxidase in the cytoplasmic membrane of *Escherichia coli*, Comp. Biochem. Physiol. C Pharmacol. Toxicol. Endocrinol. 124 (1999) 141–148.
[34] K. Kita, K. Konishi, Y. Anraku, Terminal oxidases of *Escherichia coli* aerobic respiratory chain. I. Purification and properties of cytochrome b_{562}-*o* complex from cells in the early exponential phase of aerobic growth, J. Biol. Chem. 259 (1984) 3368–3374.
[35] K. Kita, K. Konishi, Y. Anraku, Terminal oxidases of *Escherichia coli* aerobic respiratory chain. II. Purification and properties of cytochrome b_{558}-*d* complex from cells grown with limited oxygen and evidence of branched electron-carrying systems, J. Biol. Chem. 259 (1984) 3375–3381.
[36] C. Nihei, Y. Fukai, K. Kawai, A. Osanai, Y. Yabu, T. Suzuki, N. Ohta, N. Minagawa, K. Nagai, K. Kita, Purification of active recombinant trypanosome alternative oxidase, FEBS Lett. 538 (2003) 35–40.
[37] O. Maglio, F. Nastri, V. Pavone, A. Lombardi, W.F. DeGrado, Preorganization of molecular binding sites in designed diiron proteins, Proc. Natl. Acad. Sci. U. S. A. 100 (2003) 3772–3777.
[38] M.P. Hendrich, E. Munck, B.G. Fox, J.D. Lipscomb, Integer-spin Epr studies of the fully reduced methane monooxygenase hydroxylase component, J. Am. Chem. Soc. 112 (1990) 5861–5865.
[39] W.A. van den Berg, A.A. Stevens, M.F. Verhagen, W.M. van Dongen, W.R. Hagen, Overproduction of the prismane protein from *Desulfovibrio desulfuricans* ATCC 27774 in *Desulfovibrio vulgaris* (Hildenborough) and EPR spectroscopy of the [6Fe–6S] cluster in different redox states, Biochim. Biophys. Acta 1206 (1994) 240–246.
[40] M. Hoefnagel, P.R. Rich, Q. Zhang, J.T. Wiskich, Substrate kinetics of the plant mitochondrial alternative oxidase and the effects of pyruvate, Plant Physiol. 115 (1997) 1145–1153.
[41] Y. Kido, T. Shiba, D.K. Inaoka, K. Sakamoto, T. Nara, T. Aoki, T. Honma, A. Tanaka, M. Inoue, S. Matsuoka, A. Moore, S. Harada, K. Kita, Crystallization and preliminary crystallographic analysis of cyanide-insensitive alternative oxidase from *Trypanosoma brucei brucei*, Acta. Crystallogr. Sect. F Struct. Biol. Cryst. Commun, doi:10.1107/S1744309109054062.
[42] H. Miyadera, H. Amino, A. Hiraishi, H. Taka, K. Murayama, H. Miyoshi, K. Sakamoto, N. Ishii, S. Hekimi, K. Kita, Altered quinone biosynthesis in the long-lived clk-1 mutants of *Caenorhabditis elegans*, J. Biol. Chem. 276 (2001) 7713–7716.
[43] P. Stenmark, J. Grunler, J. Mattsson, P.J. Sindelar, P. Nordlund, D.A. Berthold, A new member of the family of di-iron carboxylate proteins. Coq7 (clk-1), a membrane-bound hydroxylase involved in ubiquinone biosynthesis, J. Biol. Chem. 276 (2001) 33297–33300.
[44] D.A. Berthold, P. Stenmark, Membrane-bound diiron carboxylate proteins, Ann. Rev. Plant Biol. 54 (2003) 497–517.
[45] R. Fato, M. Cavazzoni, C. Castelluccio, G. Parenti Castelli, G. Palmer, M. Degli Esposti, G. Lenaz, Steady-state kinetics of ubiquinol-cytochrome *c* reductase in bovine heart submitochondrial particles: diffusional effects, Biochem. J. 290 (1993) 225–236 K.
[46] H. Witt, F. Malatesta, F. Nicoletti, M. Brunori, B. Ludwig, Tryptophan 121 of subunit II is the electron entry site to cytochrome-*c* oxidase in *Paracoccus denitrificans*. Involvement of a hydrophobic patch in the docking reaction, J. Biol. Chem. 273 (1998) 5132–5136.
[47] Sakamoto, H. Miyoshi, M. Ohshima, K. Kuwabara, K. Kano, T. Akagi, T. Mogi, H. Iwamura, Role of the isoprenyl tail of ubiquinone in reaction with respiratory enzymes: studies with bovine heart mitochondrial complex I and *Escherichia coli bo*-type ubiquinol oxidase, Biochemistry 37 (1998) 15106–15113.
[48] M.H.N. Hoefnagel, J.T. Wiskich, S.A. Madgwick, Z. Patterson, W. Oettmeier, P.R. Rich New, Inhibitors of the ubiquinol oxidase of higher plant mitochondria, Eur. J. Biochem. 233 (1995) 531–537.
[49] R.A. Alberty, G.G. Hammes, Application of the theory of diffusion-controlled reactions to enzyme kinetics, J. Phys. Chem. 62 (1958) 154–159.
[50] R. Clifton, A.H. Millar, J. Whelan, Alternative oxidases in Arabidopsis: a comparative analysis of differential expression in the gene family provides new insights into function of non-phosphorylating bypasses, Biochim. Biophys. Acta 1757 (2006) 730–741.
[51] A.M. Wagner, K. Krab, M.J. Wagner, A.L. Moore, Regulation of thermogenesis in flowering Araceae: the role of the alternative oxidase, Biochim. Biophys. Acta 1777 (2008) 993–1000.

[52] K. Sakamoto, H. Miyoshi, K. Takegami, T. Mogi, Y. Anraku, H. Iwamura, Probing substrate binding site of the *Escherichia coli* quinol oxidases using synthetic ubiquinol analogues, J. Biol. Chem. 271 (1996) 29897–29902.
[53] T. Suzuki, T. Hashimoto, Y. Yabu, Y. Kido, K. Sakamoto, C. Nihei, M. Hato, S. Suzuki, Y. Amano, K. Nagai, T. Hosokawa, N. Minagawa, N. Ohta, K. Kita, Direct evidence for cyanide-insensitive quinol oxidase (alternative oxidase) in apicomplexan parasite *Cryptosporidium parvum*: phylogenetic and therapeutic implications, Biochem. Biophys. Res. Commun. 313 (2004) 1044–1052.
[54] C.W. Roberts, F. Roberts, F.L. Henriquez, D. Akiyoshi, B.U. Samuel, T.A. Richards, W. Milhous, D. Kyle, L. McIntosh, G.C. Hill, M. Chaudhuri, S. Tzipori, R. McLeod, Evidence for mitochondrial-derived alternative oxidase in the apicomplexan parasite *Cryptosporidium parvum*: a potential anti-microbial agent target, Int. J. Parasitol. 34 (2004) 297–308.
[55] R. Walker Jr., L. Saha, G.C. Hill, M. Chaudhuri, The effect of over-expression of the alternative oxidase in the procyclic forms of *Trypanosoma brucei*, Mol. Biochem. Parasitol. 139 (2005) 153–162.
[56] E. Vassella, M. Probst, A. Schneider, E. Studer, C.K. Renggli, I. Roditi, Expression of a major surface protein of *Trypanosoma brucei* insect forms is controlled by the activity of mitochondrial enzymes, Mol. Biol. Cell 15 (2004) 3986–3993.
[57] A. Tsuda, W.H. Witola, K. Ohashi, M. Onuma, Expression of alternative oxidase inhibits programmed cell death-like phenomenon in bloodstream form of *Trypanosoma brucei rhodesiense*, Parasitol. Int. 54 (2005) 243–251.

Acta Crystallographica Section F
Structural Biology and Crystallization Communications
ISSN: 1744-3091
Editors: H. M. Einspahr and M. S. Weiss

Crystallization and preliminary crystallographic analysis of cyanide-insensitive alternative oxidase from *Trypanosoma brucei brucei*

Yasutoshi Kido, Tomoo Shiba, Daniel Ken Inaoka, Kimitoshi Sakamoto, Takeshi Nara, Takashi Aoki, Teruki Honma, Akiko Tanaka, Masayuki Inoue, Shigeru Matsuoka, Anthony Moore, Shigeharu Harada and Kiyoshi Kita

Acta Cryst. (2010). F**66**, 275–278

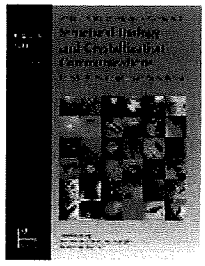

Mitochondrion 10 (2010) 158–165

Contents lists available at ScienceDirect

Mitochondrion

journal homepage: www.elsevier.com/locate/mito

Contribution of the FAD and quinone binding sites to the production of reactive oxygen species from *Ascaris suum* mitochondrial complex II

Madhavi P. Paranagama [a], Kimitoshi Sakamoto [a,*], Hisako Amino [a], Mutsumi Awano [a], Hideto Miyoshi [b], Kiyoshi Kita [a]

[a] *Department of Biomedical Chemistry, Graduate School of Medicine, The University of Tokyo, 7-3-1 Hongo, Bunkyo-ku, Tokyo 113-0033, Japan*
[b] *Division of Applied Life Sciences, Graduate School of Agriculture, Kyoto University, Sakyo-ku, Kyoto 606-8502, Japan*

ARTICLE INFO

Article history:
Received 1 May 2009
Received in revised form 22 October 2009
Accepted 9 December 2009
Available online 16 December 2009

Keywords:
Reactive oxygen species
Complex II
Ascaris suum

ABSTRACT

Reactive oxygen species (ROS) production from mitochondrial complex II (succinate–quinone reductase, SQR) has become a focus of research recently since it is implicated in carcinogenesis. To date, the FAD site is proposed as the ROS producing site in complex II, based on studies done on *Escherichia coli*, whereas the quinone binding site is proposed as the site of ROS production based on studies in *Saccharomyces cerevisiae*. Using the submitochondrial particles from the adult worms and L_3 larvae of the parasitic nematode *Ascaris suum*, we found that ROS are produced from more than one site in the mitochondrial complex II. Moreover, the succinate-dependent ROS production from the complex II of the *A. suum* adult worm was significantly higher than that from the complex II of the L_3 larvae. Considering the conservation of amino acids crucial for the SQR activity and the high levels of ROS production from the mitochondrial complex II of the *A. suum* adult worm together with the absence of complexes III and IV activities in its respiratory chain, it is a good model to examine the reactive oxygen species production from the mitochondrial complex II.

1. Introduction

The complex II superfamily comprises succinate–quinone reductase (SQR) and quinol-fumarate reductase (QFR), which catalyze the interconversion of succinate and fumarate with quinone and quinol. SQR is a component of the aerobic respiratory chain as well as the tricarboxylic acid cycle (for a review see Cecchini et al. (2002)). QFR is a component of the anaerobic respiratory chain in anaerobic and facultative anaerobic bacteria (Lancaster, 2004) and lower eukaryotes (Kita and Takamiya, 2002; Matsumoto et al., 2008; Van Hellmond et al., 2003).

SQR and QFR complexes generally consist of four subunits referred to as the flavoprotein subunit (Fp), iron-sulfur subunit (Ip), cytochrome *b* large subunit (CybL), and cytochrome *b* small subunit (CybS). The Fp and Ip subunits comprise the catalytic domain of the enzyme. The Fp subunit has an FAD as a prosthetic group and contains the dicarboxylate-binding site. The Ip subunit generally contains three iron-sulfur clusters $[2Fe–2S]^{2+,1+}$, $[4Fe–4S]^{2+,1+}$, and $[3Fe–4S]^{1+,0}$. Subunits CybL and CybS, with heme *b* as the prosthetic group, form the anchor domain of the enzyme. This anchors the catalytic domain to the inner mitochondrial membrane and also serves as the quinone oxidation/reduction site (for a review see Cecchini et al. (2002)).

Mutations in the Fp subunit in human complex II result in an infantile onset progressive neurodegenerative disease called Leigh syndrome (Ackrell, 2002; Bourgeron et al., 1995). Mutations in the Ip, CybL, and CybS subunits lead to cancers such as pheochromocytoma (tumours of the chromaffin cells in the adrenal medulla) and paraganglioma (extra adrenal tumours of sympathetic or parasympathetic origin) (Astuti et al., 2001; Bayley et al., 2006; Baysal et al., 2000; Baysal et al., 2002; Eng et al., 2003). Moreover, breast, thyroid, and renal carcinomas are associated with complex II mutations (Ni et al., 2008). However, the precise mechanism associating complex II mutations to carcinogenesis is not fully understood. Currently there are two hypotheses to explain how complex II mutations lead to carcinogenesis. One hypothesis suggests that succinate accumulation resulting from complex II dysfunction leads to stabilization of transcription factor hypoxia-inducible factor-1α (HIF-1α) by inhibiting HIF-1α prolyl hydroxylase (Briere et al., 2005; Cervera et al., 2008; Selak et al., 2005). The other hypothesis suggests that reactive oxygen species (ROS) generated from complex II defect result in oncogenesis (Guzy et al., 2008; Ishii et al., 2005). Thus, the mechanism of ROS generation from complex II has recently

Abbreviations: SQR, succinate:quinone reductase; QFR, quinol:fumarate reductase; SDH, succinate dehydrogenase; FRD, fumarate reductase; ROS, Reactive oxygen species; SOD, superoxide dismutase; SMP, submitochondrial particles.

* Corresponding author. Tel.: +81 3 5841 8202; fax: +81 3 5841 3444.
E-mail addresses: sakamok@m.u-tokyo.ac.jp, ndh1ascaris@yahoo.co.jp (K. Sakamoto).

1567-7249/$ - see front matter © 2009 Elsevier B.V. and Mitochondria Research Society. All rights reserved.
doi:10.1016/j.mito.2009.12.145